International Union of Radio Science

Modern Radio Science 1987
Edited by A. L. Cullen
Modern Radio Science 1990
Edited by J. Bach Andersen
Modern Radio Science 1993
Edited by Hiroshi Matsumoto
Modern Radio Science 1996
Edited by J. Hamelin

Review of Radio Science 1984–1986
Edited by G. Hyde (Available from URSI Secretariat)
Review of Radio Science 1987–1989
Edited by G. Hyde (Available from URSI Secretariat)
Review of Radio Science 1990–1992
Edited by W. Ross Stone
Review of Radio Science 1993–1996
Edited by W. Ross Stone

THE REVIEW OF RADIO SCIENCE 1993-1996

Edited by

W. ROSS STONE

Stoneware Limited
1446 Vista Claridad
La Jolla, California 92037-7839 USA
Tel: (619) 459-8305; Fax: (619) 459-7140
E-mail: 71221.621@compuserve.com

URSI Commission Editors
For the text:

Commission A: Motohisa Kanda
Commission B: Ralph E. Kleinman
Commission C: Paul H. Wittke
Commission D: Roberto Sorrentino
Commission E: Masashi Hayakawa
Commission F: Martin P. M. Hall
Commission G: Phil Wilkinson
Commission H: Vladimir Fiala
Commission J: Tasso Tzioumis
Commission K: James C. Lin

For the diskette of collected references:

Commission B: Anton Tijhuis
Commission E: Robert L. Gardner
Commission F: Yoshio Hosoya
Commission G: Phil Wilkinson
Commission H: Wynne Calvert
Commission K: Stefano Pisa

Published for the
International Union of Radio Science
by
Oxford University Press
1996

5. Lightwave Metrology: Optical Fibers and Power Meters

B. L. Danielson, T. J. Drapela, D. L. Franzen, S. Mechels, T. R. Scott, I. Vayshenker, and M. Young
National Institute of Standards and Technology
325 Broadway, Boulder, CO 80303 USA
Tel: (303) 497-3346; Fax: (303) 497-3387
E-mail: franzen@boulder.nist.gov

1. Introduction

The concept of long-distance lightwave communications over glass fibers was pioneered theoretically by *Kao and Hockham* [*1966*]. Researchers at the Corning Glass Works were the first to demonstrate a fiber with losses below 20 dB/km [*Kapron et al., 1970*]. This contribution was especially important, because it used a novel "soot"-vapor-deposition process, for achieving high-purity glass. Various modifications of this process are used to produce today's low-loss fiber: losses near 0.2 dB/km are routinely achieved, for wavelengths near 1550 nm.

Since 1970, the technological progress has been rapid. The first fibers to find widespread commercial use were multimode fibers that had core diameters of 50 μm. The large core diameter meant alignments could be achieved with relatively large dimensional tolerances. As the industry matured, dimensional tolerances were reduced, and low-cost connectors and splices were developed for single-mode fiber. Today, almost all long-distance lightwave communication takes place over single-mode fiber. Multimode fiber still finds use in short, local-area networks, where distances are frequently less than a few hundred meters. The evolution toward single-mode fiber was accompanied by a shift in the operating wavelength, from 800 nm to longer wavelengths. Early fiber had high levels of impurities, particularly the OH radical, which has a strong absorption at 1385 nm. One part per million of OH is enough to cause an attenuation of 39 dB/km, at 1385 nm. Modern fabrication methods have reduced the level of this impurity, so it is not a factor at wavelengths near 1300 and 1550 nm.

This chapter will review the metrology of single-mode fiber, and emphasize transmission measurements near 1300 and 1550 nm. Accordingly, the section on optical-power meters will emphasize absolute measurements at those wavelengths, and concentrate on metrology to support calibration. The presentation is mostly general, and several references are cited to provide the reader with more details. However, in some instances, specific systems and practices employed at NIST are discussed in detail. The fiber section deals with those parameters specified in commercial trade and commerce, including attenuation, mode-field diameter, dispersion, and cross-sectional geometry. A treatment of optical-time-domain reflectometry (OTDR) is included, since it is one of the most important diagnostics in field installation and fiber testing.

The optical-fiber industry is measurement-intensive. Measurements can be made during fabrication; however, most testing occurs during quality control, after the draw is complete. Further measurements may be necessary after cabling to confirm fiber performance. Finally, the fiber customer often performs measurements during incoming quality inspection. Measurements are made during system installation, to assure compliance with specifications. Also, trouble shooting and measurements to support restoration and upgrading are required, even after the system is operational. Standards have become a key issue in fiber metrology. The values obtained for any parameter can depend on the measurement method. For this reason, standards groups recommend certain methods, with specific directions for implementation. The main standards groups writing test procedures for fiber include (in the US) the Telecommunications Industry Association (TIA), and (on an international level) the International Electrotechnical Commission (IEC) and the International Telecommunication Union (ITU). There are standardized test procedures for many of the parameters covered in this chapter.

2. Optical fibers

2.1 Attenuation

Fiber attenuation is one of the most important fiber parameters. Fiber drawing results in a distribution of attenuation values, and sometimes lower-attenuation fibers bring higher prices. Attenuation measurements on single-mode fibers are not as problematic as those on multimode fibers. Effects, such as differential-mode attenuation and the subsequent concern over launching conditions, are not an issue. Since attenuation can be determined by a simple power-ratio measurement, the industry has not experienced problems in achieving the desired precision and accuracy.

Attenuation is usually measured as a function of wavelength. The main mechanism determining loss in single-mode fiber is Rayleigh scattering. It arises because of microscopic inhomogeneities that are frozen in when the glass solidifies. The attenuation coefficient due to Rayleigh scattering decreases as the fourth power of wavelength. The spectral dependence can be divided into single and bi-modal regions. For wavelengths less than what is commonly called the cutoff wavelength, both the second-order LP_{11} mode and the LP_{01} fundamental-mode are present. Near the cutoff wavelength, the second-order mode is loosely bound to the core, and exhibits high loss. Practical systems operate at wavelengths longer than cutoff, where only the fundamental mode exists.

The OH absorption occurs at 1385 nm, and divides the spectrum into two commonly used low-loss windows, near 1300 and 1550 nm. For wavelengths longer than 1600 nm, the attenuation begins to increase due to vibrational absorptions.

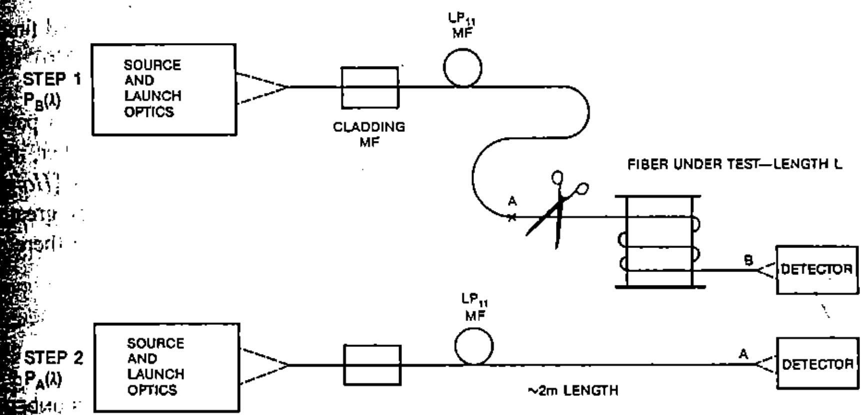

Figure 1. The two-step-cutback method for determining fiber attenuation.

The most accurate method for determining attenuation is called the "cutback" method, and is illustrated in Figure 1 [*Heitmann, 1987*]. It is a two-step procedure, where light from a tunable source is launched into the fiber under test. The source wavelength is scanned, and the relative optical power, $P_B(\lambda)$, exiting the fiber is recorded. Sometimes a mode filter, consisting of a few turns of fiber wrapped around a 2- to 3-cm-diameter mandrel, is inserted at the launch end, to further attenuate the second-order mode. Next, without disturbing the launched power, the fiber is cut 2 to 3 m from the input end, and this newly created output is aligned to the detector. The source wavelength is scanned a second time, and the relative optical power, $P_A(\lambda)$, exiting the short length is recorded. The fiber-spectral-attenuation coefficient, $\alpha(\lambda)$, in units of dB/km, is given by

$$\alpha(\lambda) = \frac{10}{L} \log\left[\frac{P_A(\lambda)}{P_B(\lambda)}\right], \quad (1)$$

where L is the remaining fiber length in kilometers.

The source for attenuation measurements is usually a quartz-halogen lamp, filtered by a monochromator (Figure 2). Light from the lamp is imaged onto the monochromator, and an order-sorting filter is inserted in the light path, to block higher-diffraction orders. The power launched into a single-mode fiber, from such an incoherent source, is lower than the power coupled into a multimode fiber. The challenge in single-mode measurements is to measure low power levels with good signal-to-noise ratio (SNR). For this reason, a lock-in amplifier is used with the detector. To achieve good power stability during the cutback procedure, a large spot size, of 100 to 200 μm, is imaged onto the single-mode fiber, whose mode-field diameter is approximately 10 μm. Thus, small movements of the fiber during the measurement will not appreciably affect the coupled power. A monitor detector can be used with the lamp, to correct for power drift during a measurement. However, if the lamp is powered by a constant-current or -voltage source, the stability is usually adequate. Proper care must be taken with the detector, to avoid potential errors. The polarization of light in the fiber may vary with wavelength and time. It is therefore important to use a detector which is insensitive to polarization. Also, the detector response must be linear, and voltage offsets in the absence of optical power must be avoided, or taken into account. It is also prudent to avoid small gaps in the fiber path: these could lead to unstable Fabry-Perot like resonances. With properly wound fiber, it is possible to obtain inter-laboratory agreement of 0.003 dB/km on 6 km lengths [*Haigh and Jones, 1994*]. The shipping package developed for those measurements greatly reduced winding stress and eliminated macrobends: environmental effects were thereby minimized.

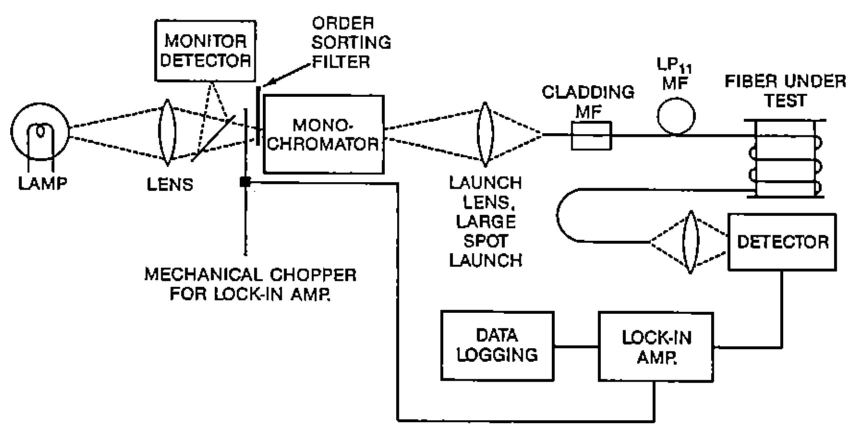

Figure 2. A typical apparatus, using a quartz-halogen lamp, for determining spectral attenuation.

Extensive use is being made of OTDR to determine fiber uniformity [*Hanson, 1993*; *Moller, et al., 1994*]. Fibers are drawn and measured in very long lengths, and subsequently cut into shorter lengths, for many applications. It is desirable to determine attenuation uniformity, so as to predict the loss of shorter lengths. Measurements with the OTDR must be taken from both ends of the fiber, and averaged, to obtain the correct result. There are algorithms for extracting the attenuation uniformity from OTDR traces [*Chiantore and Ferri, 1994*; *Artiglia, et al., 1994*].

2.2 Mode-field diameter

The mode-field diameter (MFD), describing the spatial extent of the fundamental LP_{01} mode, is important for single-mode fibers. For example, there is loss when fibers with different mode-field diameters are joined end to end. A mismatch of 10% in MFD will result in a joint loss of 0.05 dB. At wavelengths near cutoff, the radial-intensity profile is approximately Gaussian, for many index profiles in common use. Early methods of data analysis approximated the intensity distribution with a Gaussian fit. While this assumption

gave good agreement among various measurement methods on some fibers, significant differences were observed at wavelengths far from cutoff, or for dispersion-shifted fibers [*Franzen and Srivastava, 1985*]. This led to the adoption of the "Petermann-2" definition of MFD, which does not assume a functional shape for the distribution, but rather is based on moments of the electric field [*Petermann, 1983*]. The Petermann MFD, W_P, is given by

$$W_P = 2\left[\frac{2\int_0^\infty f^2(r)rdr}{\int_0^\infty \left(\frac{df}{dr}\right)^2 rdr}\right]^{1/2}, \tag{2}$$

where $f(r)$ is the electric field as a function of the radius, r. The Petermann-2 definition gives a good prediction of splice loss when fibers with different MFDs are joined, even when the distributions are not Gaussian. Moreover, when the mode field is Gaussian, the Petermann-2 definition reduces to the Gaussian.

There are a number of different techniques for determining MFD. They include transverse-offset, near-field, and far-field methods. The transverse-offset method determines MFD by measuring the transmittance of a transversely misaligned butt splice. To implement this technique, two flat, perpendicular, axially aligned fiber ends are separated by 5 μm or less, and a drop of index-matching fluid is applied to the joint. Relative transmitted power is measured as a function of transverse (radial) offset. An optical interferometer is frequently employed, to measure the displacement. The transverse-offset method is no longer in common use, whereas the near-field method is still used somewhat. The most commonly used methods are based on measurements in the far field.

2.2.1 Near-field method

The near-field (NF) method directly measures the radial-intensity variation of the fundamental mode. To implement this method, a lens, such as a microscope objective, is used, to obtain a magnified image of the fiber end [*Franzen and Srivastava, 1985*; *Anderson, et al., 1987*]. Power, as a function of radius, is typically measured, by scanning an apertured detector across the image (Figure 3). Lens magnification can be determined by imaging a pattern of known dimension. A chromium-on-glass reticule, illuminated by a fiber, has been successfully used in our laboratory. Potential errors encountered with this method include the criterion used for imaging the fiber end. An accurate implementation of the NF method employs principles of scanning confocal microscopy to focus the fiber end [*Parker, 1994*]. The NF method usually requires a laser-diode source. The apertured detector collects only a small amount of the total power exiting the fiber: consequently, there is insufficient SNR for lamp-based sources.

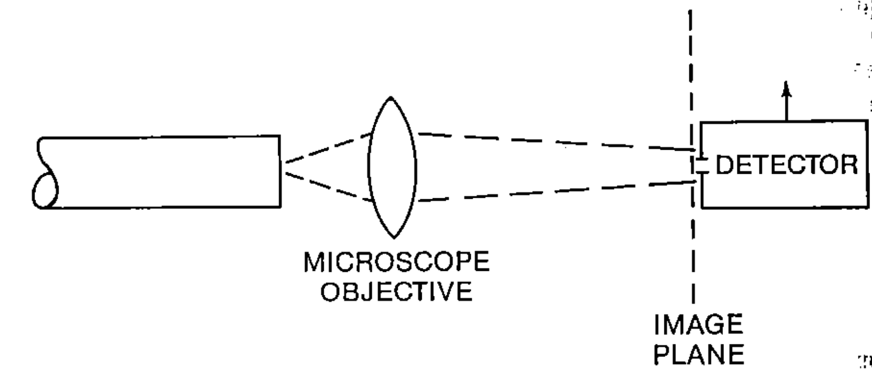

Figure 3. The near-field-scanning method for determining the mode-field diameter.

2.2.2 Far-field methods

Far-field methods are based on measurements of the angular-intensity distribution from the fiber end. Measurements are made sufficiently far from the end of the fiber to be in the far-field of the radiation pattern. The far-field of a radiating aperture is generally said to start at a distance of $10d^2/\lambda$ from the aperture, where d is the diameter of the aperture, and λ is the wavelength of the radiation. For a single-mode-optical fiber, d is approximately the MFD, and λ is commonly 1.3 or 1.5 μm. In this instance, the far-field begins a few millimeters from the fiber end, and is conveniently accessible on the laboratory bench. Far-field methods in common use are the one-dimensional-far-field (FF) and variable-aperture-far-field (VAFF) methods. After the far-field information is acquired, it is mathematically transformed to give the near-field distribution and subsequently, the MFD. In the case of fibers, the near field can be related to the far field through a Hankel transform [*Anderson, et al., 1987*; *Young and Wittmann, 1993*].

The one-dimensional far field is frequently acquired by rotating an apertured detector, so that it passes through the center of the radiation pattern (Figure 4). This can be accomplished using a precise motor-driven rotary stage. The detector is usually placed well into the far field, at perhaps $100d^2/\lambda$. The FF method is extremely simple, since the beam interacts with no optics, and calibration of the system requires only the angular spacing between data points. As a typical example, a detector aperture of 200 μm, placed 10 cm from the fiber end, gives an adequate angular resolution of 0.1°, and the radiation pattern is recorded to 40 or 50 dB below the peak intensity. The angular range required depends on the type of fiber: dispersion-shifted fibers, having smaller MFDs, requires a larger scan angle [*Klemas, 1985*].

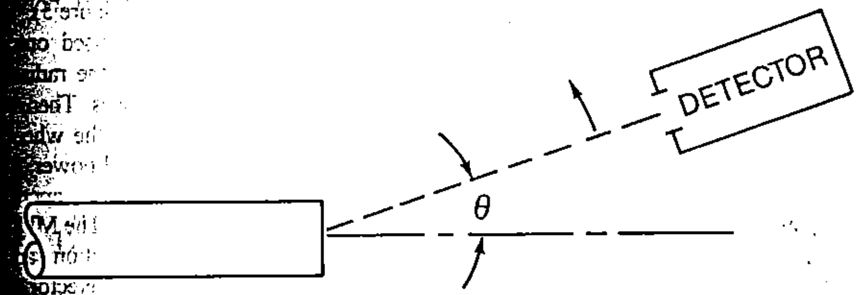

Figure 4. The one-dimensional far-field-scanning method (FF), for determining the mode-field diameter.

In the case of a Gaussian mode-field distribution, the relation between the near and far fields is very simple, since the transform of a Gaussian yields another Gaussian. For this special case, the MFD calculated from the far-field distribution is given by

$$W_{FF} = \frac{2\lambda}{\pi \tan\theta}, \tag{3}$$

where θ is the angle where the far-field distribution has decreased by $1/e^2$. As with the NF method, the apertured detector collects a small portion of the power exiting the fiber: therefore, a source such as a laser diode is required for adequate SNR.

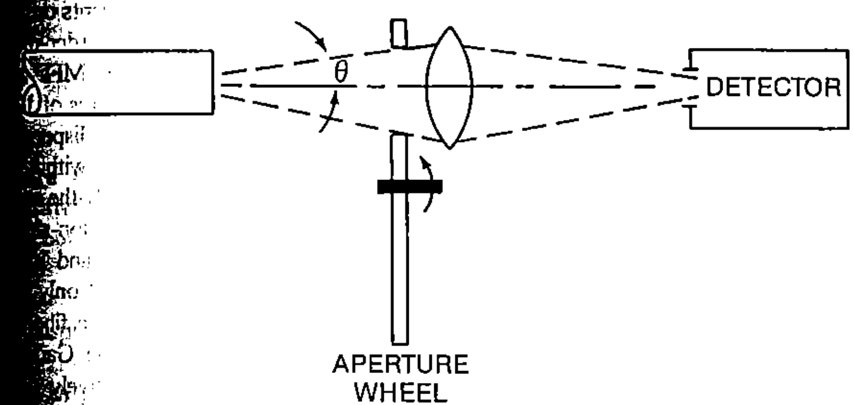

Figure 5. The variable-aperture-far-field method (VAFF) for determining the mode-field diameter.

In the common implementation of the variable-aperture-far-field (VAFF) method, an aperture wheel, containing 12 to 20 apertures, is placed in the far field (Figure 5). The power transmitted through the apertures is collected by a lens, and focused onto a detector. Some method of initial alignment is usually employed to center the radiation pattern on the first aperture, to allow for slightly non-normal fiber-end faces. Then, the relative power passing through the apertures is sequentially measured, as the wheel is rotated: usually one aperture is large enough to collect all of the transmitted power. The power collected in various cone angles is determined by measuring the aperture diameters, and the distance from the wheel to the fiber, which remains fixed. The MFD is found by fitting a mathematical expression to the data: the Petermann-2 definition can be transformed to the far-field [*Pask, 1984*]. Errors are encountered when the detector fails to collect all of the power transmitted through the apertures, because of aberrations in the lens. This is especially critical for dispersion-shifted (DS) fibers, which have relatively small mode-field diameters and, therefore, wide-angle-radiation patterns. For example, a VAFF system, with a collection numerical aperture (NA) of 0.2, can give a 7% error for some types of DS fiber [*Parton, 1988*]. This error was eliminated through the use of mirror optics, which increased the collection NA to 0.4 [*Parton, 1988*]. The VAFF method collects a larger fraction of the power exiting the fiber than FF scanning. Therefore, it is possible to achieve acceptable SNRs using an incandescent lamp and filter. The same source as is used for spectral-attenuation measurements (Figure 2) can be used with a VAFF system.

2.2.3 Interlaboratory Comparisons

NIST participated with members of the TIA to evaluate far-field methods for determining MFD [*Drapela, 1988*]. The comparison used six single-mode fibers, two dispersion-shifted and four dispersion-unshifted. Participants made measurements on 2 m lengths, with a single 50 mm diameter loop, to strip out possible second-order-mode power. Seven participants submitted results using FF, while five used VAFF. MFD was determined using both the Gaussian and Petermann-2 definitions, at wavelengths of 1300 and 1550 nm. The results could be categorized into three groups: 1300 nm dispersion-unshifted, 1550 nm dispersion-unshifted, and dispersion-shifted. For fibers within the same group, the relative differences between FF and VAFF were approximately the same. In this study, the nominal values of MFD ranged from 7 to 12 μm, with dispersion-shifted fibers having the smallest diameters. For unshifted fibers at 1300 nm, the FF and VAFF methods agreed well for the Petermann-2 definition, with an average offset of only 0.04 μm; agreement with the Gaussian was not as good (0.28 μm). For the same fibers at 1550 nm, where the mode profiles are not as Gaussian, the offset for the Gaussian definition was 0.59 μm, whereas the Petermann agreement was still relatively good (0.05 μm); results for one of the fibers are shown in Figure 6. The largest offsets of all were encountered for the DS fibers. Here, the mode profiles are even further from a Gaussian shape, and a large disagreement of 0.52 μm was observed, even with the Petermann-2 definition. The large FF/VAFF offsets in this case are due to the small mode-field diameters of the DS fibers. If the VAFF collection optics truncates the far-field-radiation pattern, this translates into a larger measured MFD. Measurements on the

DS fibers, using a VAFF with 0.4 NA collection, reduced the FF/VAFF offset to 0.07 μm [*Parton, 1988*].

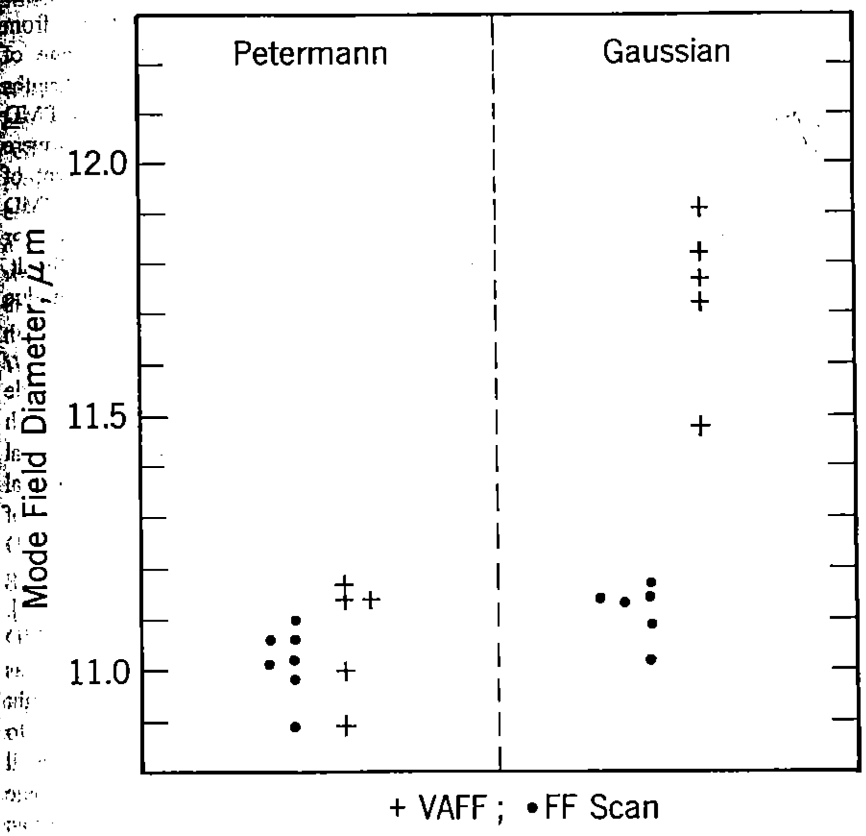

Figure 6. The results of an interlaboratory comparison (fiber 4, dispersion unshifted, 1550 nm), to determine mode-field diameter using far-field methods, with both Gaussian and Petermann definitions.

2.3 Dispersion

Dispersion results when different wavelengths or different modes propagate in the fiber with different group velocities. This causes temporal broadening of light pulses, and in practical systems, sets limits on the bit rate. Dispersion is commonly attributed to either polarization or chromatic effects.

2.3.1 Polarization-mode dispersion

Polarization-mode dispersion (PMD) occurs when different polarization states travel with different group velocity. In standard fiber, this is caused by non-intentional core deformation, introduced when the fiber is fabricated, and external stress, from cabling or the environment. PMD values are typically small, and in the range of 0.1 ps/km$^{1/2}$. For short lengths, PMD scales linearly with length. However, for lengths long enough to result in significant power coupling between polarization states, PMD scales as the square root of length. In early terrestrial applications, repeater spacings were not long enough to result in appreciable PMD. However, with the development of optical-fiber amplifiers, the optical lengths can exceed thousands of kilometers, and PMD can be an issue in submarine systems, especially at higher bit rates. The statistical behavior of PMD in standard telecommunications fiber makes the measurement difficult. Differential-group delay between polarization states in long fibers changes with time, due to small changes in the environment.

Three common methods, used to characterize PMD in long fibers, include wavelength scanning, Jones-matrix eigenanalysis (JME), and interferometry. Wavelength scanning consists of placing the fiber between polarizers, and measuring the spectral transmittance [*Poole and Favin, 1994*]. The spectral transmittance exhibits several maxima and minima. More extrema over a given spectral range indicate higher values of PMD. Data-handling algorithms, to quantify the number of extrema from which the PMD is calculated, have been developed. An interlaboratory comparison was conducted among TIA members, to evaluate the wavelength-scanning method [*Gardner, 1994*]. Measurements on two 5 km fibers showed that the statistical variation of PMD significantly affected the results. For one of the fibers, the mean value of PMD was 0.107 ps/km$^{1/2}$, with a measurement spread (one standard deviation) among eight participants of 0.026 ps/km$^{1/2}$. In the Jones-matrix method, a polarimeter is used to measure the output polarization as the input wavelength and polarization are varied [*Heffner, 1992*]. JME gives instantaneous PMD as a function of wavelength; an average PMD value can be extracted from this measurement. The interferometric method uses an incoherent source, such as a light-emitting diode (LED). The fiber output is analyzed with a Michelson interferometer, to determine the autocorrelation function and resultant mean PMD value [*Gisin, Von der Weid, and Pellaux, 1991*].

2.3.2 Chromatic dispersion

Chromatic dispersion arises because different wavelengths exhibit different group velocities. Pulse broadening therefore results, because of the finite source-spectral width. Of interest in optical fibers is the dispersion coefficient, $D(\lambda)$, which is the derivative of the group delay, $T(\lambda)$, per unit fiber length: that is, $D(\lambda) = dT(\lambda)/d(\lambda)$. D is usually expressed in units of ps/(nm·km). In optical fibers, chromatic dispersion is composed of both material and waveguide effects. The material part is due to the spectral variation of the bulk refractive index, and is given by

$$D_{mat} = -\frac{\lambda}{c}\frac{d^2 n}{d\lambda^2}, \qquad (4)$$

where n is the refractive index, and c the speed of light.

The waveguide contribution arises from the change in mode profile with wavelength. As wavelength increases, more of the power is carried in the cladding, which has a lower index of refraction than the core. Thus, the mode experiences a net "effective" index of refraction which changes with wavelength. The total dispersion properties of the fiber can be altered by changing the waveguide dispersion. The most common types of dispersion behavior have been classified by the TIA (formerly the EIA), and are illustrated in Figure 7. In dispersion-unshifted fiber, the zero-dispersion wavelength is near 1310 nm, and results principally from material dispersion. For dispersion-shifted class IVb fibers, the waveguide dispersion has been increased to move the net zero dispersion to 1550 nm, to coincide with the lowest-loss wavelength. Waveguide dispersion is controlled by the shape of the index-of-refraction profile.

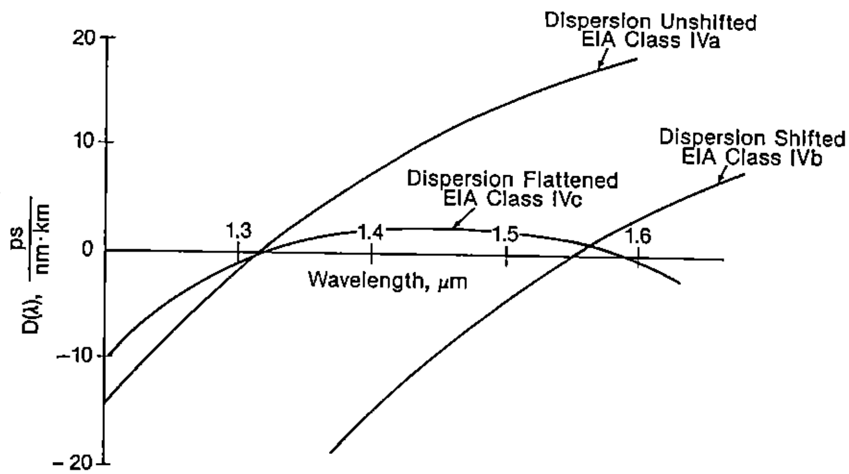

Figure 7. The dispersion classes of single-mode fiber, according to the EIA/TIA standards group.

Measurement techniques, to determine chromatic dispersion, can be classified into time- or frequency-domain methods. The earliest measurements employed pulsed-laser diodes at a discrete number of wavelengths, or a continuously tunable fiber-Raman laser [*Cohen and Lin, 1978*]. The Raman laser uses a high-power, Q-switched, mode-locked Nd:YAG laser, at 1.06 μm, as a pump source. Pulses from the pump are launched into a few hundred meters of single-mode fiber. Stimulated Raman scattering yields a wavelength continuum from 1.1 to 1.7 μm. A continuously tunable source, with a pulse duration of 50 ps, results from filtering the Raman light with a monochromator. As the source is tuned, a sampling oscilloscope is used to measure the propagation delay as a function of wavelength. Finally, the dispersion coefficient is found by curve-fitting the group delay and differentiating.

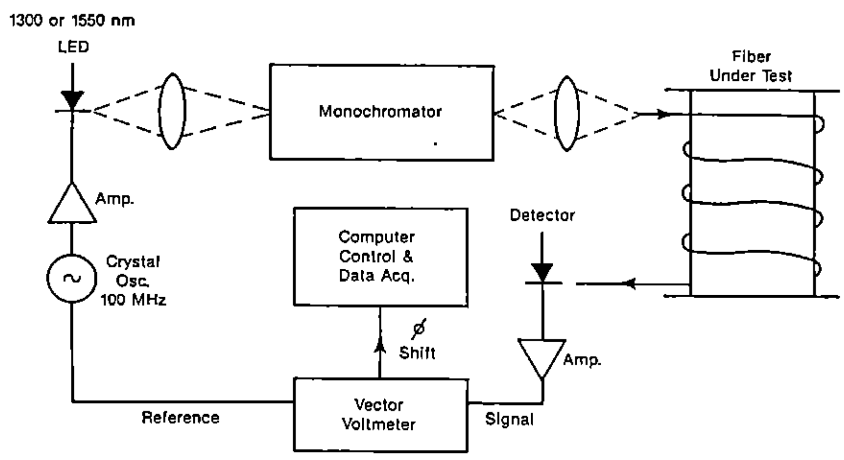

Figure 8. The frequency-domain technique, using a filtered LED to determine chromatic dispersion.

More recent methods are based on frequency-domain techniques. One common method is shown in Figure 8 [*Costa, et al., 1982*]. A light-emitting diode (LED) source is sinusoidally modulated, typically at 100 MHz, and filtered by a monochromator. The light is launched into the fiber under test, and the detected output goes to the signal port of a vector voltmeter. A portion of the electrical sinusoidal drive to the LED is connected to the vector voltmeter reference port. The monochromator is tuned, and the relative phase shift of the detected signal is recorded as a function of wavelength. Since phase shift is related to time delay, the group delay, $T(\lambda)$, can be determined. This method finds common use, since LEDs are much more compact and cost effective than high-power lasers. In addition, the equivalent time resolution is superior to that of oscilloscopes. A modification of this method uses the same approach, but with a differential detection scheme [*Barlow and Mackenzie, 1987*]. In this case, the monochromator wavelength is modulated at a low frequency, and differential detection is accomplished with a phase detector and lock-in amplifier. With this approach, the dispersion coefficient is directly measured, without the need for acquiring the group delay, curve fitting, and differentiating.

NIST is developing a dispersion-measurement system with improved accuracy, which will be used to calibrate reference fibers for zero-dispersion wavelength. The system, being developed by S. Mechels, and based on the frequency-domain phase-shift technique, is shown in Figure 9. The source is a grating-tuned laser diode, in either the 1300 or 1550 nm spectral region. Laser intensity is modulated by a lithium-niobate integrated-optical modulator. To improve time resolution, the modulation frequency is increased to 2 GHz. The vector voltmeter has a resolution of 0.1°, giving a time resolution less than 0.2 ps. The wavelength of the laser diode is determined interferometrically by a wavemeter, with a HeNe-laser reference. Repeated measurements

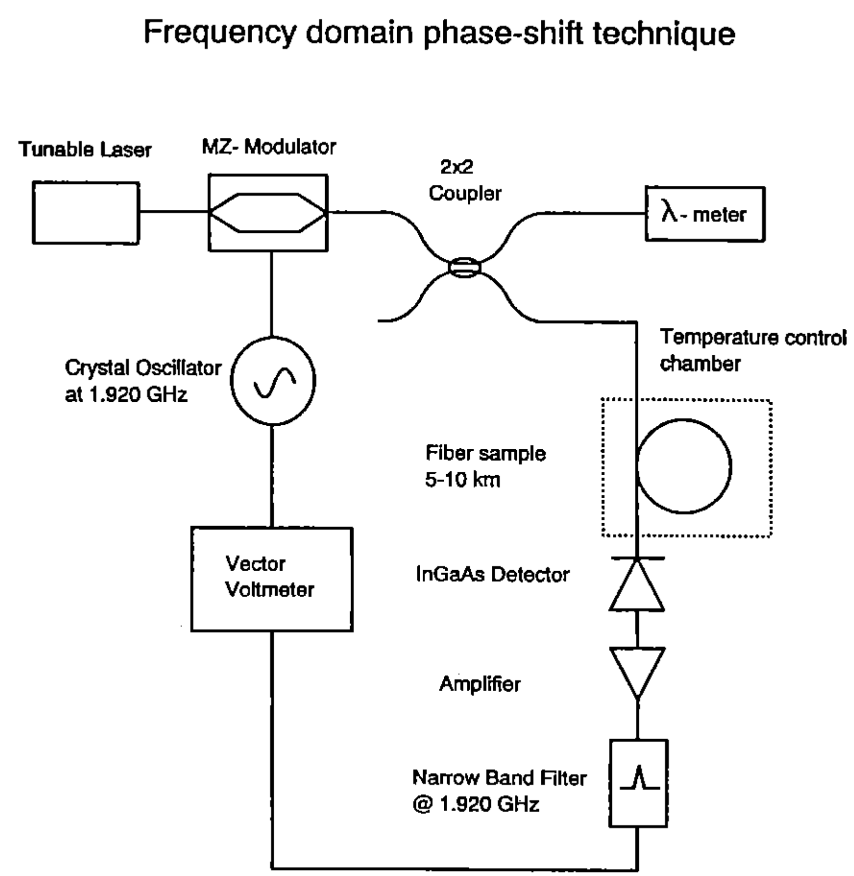

Figure 9. A high-accuracy frequency-domain technique for determining chromatic dispersion, based on a narrow-linewidth, grating-tuned laser-diode source, modulated by an integrated-optic modulator, and using a wavemeter to determine wavelength.

of the zero-dispersion wavelength, on 8 km fiber lengths over a period of a few hours, exhibit a spread (three standard deviations) of 0.1 nm or less. Of interest is the long-term stability of packaged reference fibers. Measurements on one 8 km fiber, taken over a 10 month period, indicate a stability in the range of 0.1 to 0.2 nm. Studies are continuing, to determine the nature of the long-term fluctuations.

2.4 Geometry

Fiber geometry is the term used by the TIA as a catch-all term, to describe the mean diameter of a fiber, its noncircularity, and the decentering (or concentricity error) between the center of the core and the center of the cladding. Geometry can be determined using TIA procedure FOTP-176, "Method for measuring optical fiber cross-sectional geometry by automated gray-scale analysis," or a corresponding "IEC geometry calibration procedure." Geometrical parameters are usually measured with a video microscope or gray-scale system that digitizes the image of a cleaved fiber end.

Measurements of noncircularity and decentering do not require absolute accuracy, but cladding diameter must be measured within 0.1 μm or so, in order to manufacture efficient connectors that do not require manual adjustment. Measurements made with video microscopes, however, may well suffer from a systematic error of a few tenths of a micrometer [*Mechels and Young, 1991a*]. The TIA therefore requested that the national standards laboratories develop an artifact standard, for calibrating cladding-diameter measurements. The subcommittees were, however, reluctant to accept any standard other than an optical fiber, because the measured result is a function of illumination, and because reflection from a metal film displays phase shifts that are not present in reflection from a glass edge [*Baines, et al., 1990*].

In this section, we describe the gray-scale system, and several methods used to measure the cladding diameter absolutely [*Young et al., 1993*]. We will continue with a description of a contact micrometer that NIST used to develop a Standard Reference Material, that is, a fiber whose diameter is accurately measured, and offered for sale as a traceable standard. The uncertainty of the measurement is quoted as 40 nm (here and throughout Section 2.4, uncertainty always means three standard deviations of the mean). We will conclude with a brief description of ferrule and coating measurements.

2.4.1 Video microscopy

The video microscope, or gray-scale system, typically consists of a microscope, an illuminator, and a television camera. In one realization, used at NIST, the cleaved fiber end emerges from a hole in a white diffusing screen [*Brillant et al., 1994*]. The screen is illuminated with a ring illuminator that is concentric with the microscope objective. The light that is reflected by the screen backlights the fiber, so the image appears as a black disk on a bright background. Some commercial instruments use a set of light-emitting

diodes, instead of the ring illuminator. Others illuminate the end of the fiber through the microscope objective, by means of a beam splitter located within the body of the microscope.

The system used at NIST, for example, uses a closed-circuit-television camera and a frame-digitizing plug-in board in a computer. The image is digitized as an array of 512 × 440 pixels. (This array is approximately square, since the pixels themselves are not square.) The edge of the image of the cladding is a few pixels wide. It is located by scanning a row or a column and calculating, for example, the inflection point or a fixed intensity, such as the intensity that is midway between the black inside of the image and the white outside. The locus of such points is called an edge table. If the fiber end is perfect, that is, has no dirt or defects, the edge table is approximately an ellipse. Otherwise, most of the points lie on an ellipse, but there are a significant number of outliers.

The diameter and noncircularity of the cladding are calculated by fitting a curve to the edge table. The curve that is fitted may be an ellipse or a cubic spline, for example. In either case, it may be necessary to eliminate the outliers before settling on a final fit. The group at NIST has developed a method that eliminates the outliers by robust regression: Their program calculates the least *median* of squares, rather than the least *sum* of squares, in order to filter outliers [*Wang, et al., 1994*]. Then, to save computing time, they fit an ellipse to the remaining data set by least sum of squares. Many other schemes for rejecting outliers either require the intervention of the operator, or discard good data as well as outliers.

When the light is partially coherent, as in a microscope, it is difficult to locate the geometrical image of an edge accurately. If the scale is calibrated, the *distance* between two isolated lines or points can be measured accurately, but there may be an error of a few tenths of one micrometer in measuring the *width* of an extended object and, therefore, in measuring the cladding diameter. It is for this reason that the national standards laboratories have developed traceable standards. These standards are used to calculate an additive correction to the raw measurement made in the video microscope. When the standards are used, the disagreement among laboratories decreases markedly [*Drapela et al., 1994*].

The core of the fiber may be illuminated separately. The core of most telecommunications fibers is multimode, at the wavelengths used in video microscopy (typically either 550 nm or approximately 850 nm), but this seems to present little problem, as long as the core is overfilled and, therefore, uniformly illuminated. The center of the core may be calculated from a fitted curve, in much the same way as the center of the cladding. In principle, the distance between those centers is the decentering of the core, a number that may be important for "connectorizing" the fiber. In fact, however, there is a small systematic error of unknown origin, and it is necessary to correct for this error empirically [*Brilliant et al., 1994*].

The video microscope has also been used for coating-diameter measurements [*Hallam and Shaw, 1992*]. It is difficult (though not impossible) to cleave a coated fiber so that the fiber and the cladding can be viewed end-on, so these measurements are usually made with the fiber held transversely to the axis of the microscope. The fiber is held in a small cell, filled with index-matching fluid. Then, if the match is fairly close, it is possible to view the inner coating (if the fiber is doubly coated), the cladding, and the outside of the coating. Measurements are one-dimensional, but the fiber must be rotated through 180°, in increments of 30° or 45°, in order to measure parameters such as noncircularity and the decentering of the fiber with respect to the coating center (see Section 2.4.6, below).

2.4.2 Interferometry

Fizeau interferometers were among the first instruments used to measure cladding diameter absolutely [*O'Sullivan and Gransden, 1987*; *Emig, 1990*]. The measurement can be made with a single wavelength, if the fiber is laid on an optical flat, and another flat is placed on top of the fiber with one end resting against the first flat. If the wavelength is known, the diameter of the fiber may be calculated from the total number of interference fringes between the point where the top flat contacts the fiber and where it contacts the bottom flat. The uncertainty of the method is limited to perhaps 150 nm by the difficulty of locating the contact points, and of interpolating between fringes.

White-light-interference microscopy has proven more fruitful [*Saunders, 1988; Emig, 1990; Hale and Franzen, 1992*]. A microscope is fitted with a Michelson interferometer attachment, or a Mirau interference objective, and a broad-band illuminator. The fiber, in a transverse position, is illuminated from above, through the objective lens: that is, the periphery of the fiber, not the end, is imaged onto the video camera. Because of the bandwidth of the illumination, interference fringes are visible only when the instrument is focused very near to a reflecting surface, and the fringes are strongest when the surface is precisely in focus. Thus, as the stage is translated parallel to the axis of the microscope, short bursts of interference fringes will appear as surfaces come into and go out of focus. The diameter of a fiber is measured by finding the centers of the bursts of fringes from the top and bottom surfaces of that fiber.

The group at NIST chose a Mirau objective over the Michelson interferometer because of its stability, ease of operation, and higher magnification [*Hale and Franzen, 1992*]. The system consists of a commercial metallurgical microscope, with bright-field illumination and a video camera. An optical flat is held parallel to the Mirau objective, and the fiber is held against that flat by a semi-circular brass weight that contains a slot, through which the fiber and flat are viewed. The axial position of the flat is monitored with a heterodyne interferometer that has a least count of approximately 1/500 fringe, or about 1.25 nm. The white-light fringes are monitored with a video analyzer.

Measurements are made by observing white-light fringes from the top of the fiber, and then from the flat. If the fiber is not removed, the random uncertainty of a set of measurements is about ±10 nm; the uncertainty increases to ±25 nm, when the fiber is removed and replaced between measurements.

Other groups have attempted to use Lloyd's mirror and similar arrangements to measure cladding diameter [*Wanser and Anderson, 1991*; *Joenathan and Bunch, 1993*], and there have been attempts to use the interference fringes caused by scattering or backscattering as well [*van der Mark and Bosselaar, 1994*; *Baines, Freehill, and Raine, 1994*; *Brehm et al., 1994*; *Frins et al., 1994*]. In particular, a group from the National Physical Laboratory (NPL), in the UK, calculated backscattering patterns and compared them with measured patterns, in order to estimate the diameter of the fiber. They had to adjust both the index of refraction and the diameter as part of their calculation. They estimated an uncertainty of about 70 nm. The uncertainty was somewhat larger for an elliptical fiber.

2.4.3 Confocal microscopy

Groups at NIST and NPL have constructed stage-scanning confocal microscopes that use a heterodyne interferometer to measure position [*Mechels and Young, 1992*; *Mechels and Young, 1991b*; *Collyer et al., 1991*]. The image in a confocal microscope is highly coherent, unlike that in a conventional video microscope. We can therefore find the true location of an edge either by calculating the amplitude image and seeking its inflection point or, equivalently, by finding the 25 % intensity point (the point where the intensity is 25 % of the intensity when all of the light reflects off the specimen).

To help assess the accuracy of the confocal microscope as an absolute measuring device, the group at NIST first measured widths of chromium-on-glass lines that had previously been calibrated by NIST's laboratory in Gaithersburg [*Mechels and Young, 1991b*]. Their measurements agree with the Gaithersburg measurements within about 30 nm, though the sign of the disagreement depends on whether the line is clear or reflecting. The NIST group further experimented with changing the diameter of the pinhole before the detector. Theory suggests that the pinhole diameter should be less than one-half the Airy-disk radius in the plane of the pinhole; if not, the image is equivalent to an image in partially coherent light, and the apparent position of the edge is shifted measurably. The NIST group showed that a systematic error can arise if the pinhole is larger than the value suggested by theory. They measured diameters of carefully cleaved fibers, and found a random uncertainty of 40 nm.

2.4.4 Contact micrometry

Mechanical-contact micrometers have been improved to provide low-enough uncertainty for reference measurements of fiber-cladding diameter [*Smithgall and Schroeder, 1980*; *Young et al., 1993*]. The contact micrometer used at NIST consists of a stationary, cylindrical *anvil*, and a flat, moving *spindle* [*Young et al., 1993*]. Both are steel or vitreous silica, and have been polished with hard laps in an optical shop. The spindle is aligned so that the polished end is accurately parallel to the anvil. It rides horizontally on an air bearing, and is pressed against the fiber with a known force. Its position is measured by a heterodyne interferometer.

The fiber and the anvil are held at right angles to each other, so they make contact at a point. Owing to the force with which the fiber is pressed against the anvil, there is measurable compression at that point. The compression depends on the elastic constants of the materials and can, in principle, be calculated from a standard formula. The calculated value is then used as a correction to the measurement. Because the fiber is flexible, however, it curls around the spindle, and undergoes more compression than that calculated by the formula, probably because it does not lie flat against the spindle. The compression does, however, display the correct functional dependence on force: force to the two-thirds power. Therefore, instead of relying on the compression calculated by the formula, the group measured the diameters of a number of fibers as a function of force, plotted the data as a function of force to the two-thirds power, and extrapolated to zero force, in order to estimate the diameters in the absence of force. All the fibers they tested gave the same slope, within experimental uncertainty, so, once that slope was determined, a fiber's diameter could be measured with a single measurement at a single known force. The uncertainty of the measurement was estimated as approximately 40 nm.

The NIST group intercompared its three instruments. They estimate the overall uncertainty of the micrometer as 50 nm; of the confocal microscope as 40 nm; and of the white-light-interference microscope as 30 nm. The interference microscope and the micrometer agree within a few nanometers, on average, whereas the confocal microscope may display a systematic error of 20-25 nm. The cause of the systematic error is unknown. The microscopes are hard to use, so the micrometer, having been verified by the other instruments, is the workhorse with which NIST calibrates standards.

Laser-scanning micrometers have also been used for fiber-diameter measurements. These are devices that scan a laser beam in angle across the specimen. A detector is located behind the specimen, and measures the angle over which the specimen eclipses the beam or, equivalently, the time during which the specimen eclipses the beam. These micrometers are not absolute measuring devices, however, and must be calibrated. A similar instrument has been used to examine the coatings of a fiber immersed in an index-matching fluid (see Section 2.4.6, below).

2.4.5 Traceable standards for cladding diameter

NIST offers a Standard Reference Material (SRM) for cladding diameter. It consists of a small housing that contains a retractable plunger. A fiber protrudes a few millimeters from the plunger, and may be retracted wholly inside the housing for protection; it is pushed outside the housing only when a measurement is required. The end of the fiber has been carefully cleaved, so that the end face is undamaged, and perpendicular to the axis of the fiber. The SRM is designed for calibrating video microscopes, and has an estimated uncertainty of 42 nm. The SRM, available as SRM 2520, can be obtained from the National Institute of Standards and Technology, Office of Standard Reference Materials, Room B311, Chemistry Building, Gaithersburg, Maryland 20899 USA.

NPL provides three types of artifacts: a chromium-on-glass annulus, the mean diameter of which is about 125 μm; a disk of similar diameter; and a fiber. The annulus is a reflecting annulus on a clear background: it is 10 μm wide, and is used for calibrating the scale of a video microscope. An annulus can be used to calibrate the length scale of the microscope, but not to correct for the systematic error of a width or diameter measurement. This is so because any radial scan across the annulus encounters two edges that face each other. Provided that the microscope is position-invariant across 10 μm, the systematic errors from the two edges cancel each other, and a measurement of the mean diameter of the annulus is accurate. The NPL artifacts can be obtained by contacting Optical Fibre Measurements, Division of Mechanical and Optical Metrology, National Physical Laboratory, Teddington, Middlesex, TW11 0LW, UK.

For correcting the systematic error, NPL supplies two chromium-on-glass disks. One is a reflecting dot on a clear background; the other is a clear circle on a reflecting background. It is sometimes tricky to use such artifacts in a system that is designed for imaging fiber ends, so NPL also supplies an unmounted fiber the end of which is certified within 150 nm (NPL specifies 100 nm, 2 standard deviations). NPL's artifacts are calibrated using a high-resolution video microscope that has been calibrated against a confocal microscope and a backscattering measurement.

2.4.6 Ferrule and coating geometry

Ferrule geometry is more complex than fiber geometry. In addition to the outside diameter and noncircularity, and the diameter and decentering of the hole, designers are concerned with the tapers of both the outside diameter and the hole, and with the parallelism of the hole to the axis of the ferrule itself. The inside diameter of the hole is assessed (rather than measured) by passing fine steel wires, or pin gages, through the hole. If the diameters of the pin gages are known accurately enough, the diameter of the hole can be approximated by a "go–no-go" measurement.

NIST has used the contact micrometer to measure pin-gage diameter with roughly the same uncertainty as fiber diameter. NIST intends to supply an SRM for pin-gage diameter.

Likewise, NIST has built additional micrometers that have tungsten-carbide contacting surfaces, rather than silica or steel. These carbide surfaces are needed because most ferrules are made of cubic zirconia, which is harder than silica or steel, and may damage those materials. The harder surfaces also reduce the deformation. Measuring the diameter of a ferrule with such a micrometer is more complicated than measuring the diameter of a fiber or a wire. The graph of measured diameter as a function of force to the two-thirds power is not well-fitted by a line, but rather by a parabola, probably because of the hole in the center of the ferrule. Nevertheless, if the parabolic fit is not extrapolated too far, the diameter may be measured by extrapolating to zero force. As of this writing, NIST intends to offer an SRM of ferrule outside diameter and noncircularity. The noncircularity will be measured with a precision-roundness-measuring machine, the spindle errors of which are well characterized, and allow deviations from circularity to be measured with an uncertainty of 24 nm.

Finally, NIST is working with Corning, Inc., and NPL, to develop an SRM for coating diameter [*Cooper and Hepburn, 1993*; *Smith, 1990*]. The current specification of coating diameter is 245 ± 10 μm, but the industry hopes to reduce the uncertainty to 5 μm by using a standard.

Fibers are coated with polymers–sometimes, two layers of polymer–in order to protect the fibers themselves from the environment. The inner layer is soft, and protects the fiber from microbending, whereas the outer layer is harder, and gives the coating strength. The outer diameter of the coating and the decentering of the cladding are important, for example, in designing ribbon cables and connectors. The diameter of the inner layer of the coating may likewise be important to the manufacturer. These properties are usually measured by a side-viewing method, either video microscopy or transverse scanning of a laser beam. Transverse scanning is too complicated and specialized to describe here in detail [*Marcuse, 1981*]; let it suffice to say that a laser beam is focused onto the fiber and the fiber is scanned across the beam. If the outer layer has a different index of refraction from the immersion fluid, there will be a sudden change of the deflection of the beam as it crosses the boundary between the fluid and the coating. Likewise, there will be a sudden change of the deflection at the interface between the inner and outer coating layers. Careful study of the deflection function can reveal the diameters of the outer and inner coatings and of the cladding. Like video microscopes, however, scanning systems are not absolute measuring devices and must be calibrated, presumably by an artifact standard.

Fiber coatings may well be attacked or altered by the index-matching fluids used in gray-scale or other systems. In consequence, the TIA has advised that the standard be made of a glass rod that has the appropriate diameter, and an index of refraction approximately equal to that of typical coatings. Preliminary experiments have been successful, and NIST plans to offer a glass-rod SRM as soon as satisfactory rods can be obtained.

2.5 Optical reflectometry

Optical reflectometry is used for the characterization of optical-fiber systems and components. This method can trace its origin to the development of the optical-time-domain reflectometer (OTDR) by *Personick* [*1977*] and *Barnoski et al.* [*1977*]. Since that time, reported OTDR applications have spanned the range from length determinations of fibers over 100 km long to structure analysis in optical circuits with length scales of a few millimeters. Other specific measurement examples include

determination of fiber attenuation, break location, diameter fluctuations, splice quality, mode conversion at joints, defect identification, and microbending loss. Most of these applications are associated with testing long-distance (many kilometers) optical-telecommunication systems.

Our interest here is with recent developments in optical reflectometry. For the most part, these have occurred in experimental high-resolution techniques. These applications are concerned with short-range optical-fiber systems (a few hundred meters or less), and with the nondestructive evaluation of optical components and optical-integrated circuits, the optical path lengths of which are the order of centimeters. Historically, these high-resolution techniques evolved from the OTDR systems developed for diagnostics on long-haul fiber systems. Of the many experimental techniques currently available, optical-low-coherence reflectometry (OLCR) is now favored, in applications where the ultimate in high resolution is required. Here, spatial resolutions of a few micrometers are routine. We will review the recent advances in OLCR, and some of the other high-resolution methods, which have been reported in the literature. Finally, we will discuss a novel OLCR method for the determination of group index in optical fibers. The group index plays an important role in measuring distances accurately by reflectometry.

2.5.1 Reflectometry techniques: time domain

A recent survey article [*Galtarossa et al., 1993*] has described in some detail most of the more significant reflectometry techniques. We mention here some additional new advances, not included in that reference, which address special aspects of high-spatial-resolution reflectometry. For our purposes, we define high resolution, in general terms, as the ability to spatially discriminate between reflecting events separated by a few centimeters or less.

Conventional OTDR, which uses short-duration optical pulses as a probe, is the archetype of most subsequent reflectometry techniques. It is analogous to pulsed radar, and can be applied to fiber and other guided-wave transmission systems. There is, however, the important distinction that OTDR can gather information from distributed scattering, as well as discrete reflections. The spatial resolution of this system is defined as the smallest spacing, Δx, between scattering centers that can just be resolved, and is given by

$$\Delta x = \frac{cW}{2N}, \qquad (5)$$

where W is the duration of a rectangular optical pulse, c is the velocity of light, and N is the group index of the optical waveguide. This relation assumes that the bandwidth of the receiver is large compared to $1/W$. One problem with this definition is that interference can occur between two reflected pulses which occur in close proximity, but certain experimental techniques can compensate for these effects.

It is a characteristic of all reflectometry techniques that reflected power (from a discrete region) is proportional to probe-pulse power, but that the Rayleigh-scattered signal power (from a distributed region) is proportional to the energy in the probe pulse. The short-duration pulses, necessary for high resolution, are usually associated experimentally with low energies. Although this makes detection of backscattering difficult due to small signals, OTDR backscattering has been observed in some integrated-optical devices with a spatial resolution about of 100 μm.

While highly successful and widely used, the pulsed-high-resolution OTDR systems are being supplanted by other methods discussed below. This is largely because the superior performance from these newer techniques can be obtained with less instrumental complexity, smaller size, and at lower cost.

2.5.2 Reflectometry techniques: photon counting

This method, sometimes called single-photon optical-time-domain reflectometery (SP-OTDR), uses special Geiger-mode avalanche-photodiode detectors to improve both sensitivity and resolution. It is capable of spatial resolutions in the range of 0.5-1 cm [*Ripamonti et al., 1993*].

2.5.3 Reflectometry techniques: frequency domain

Optical-frequency-domain reflectometry (OFDR), as the name implies, uses frequency modulation rather than intensity modulation of the probe light. There are basically two types of OFDR. The first involves RF amplitude-modulation of a CW source, in which the modulation is frequency-swept. Reported spatial resolutions are about 3-4 cm [*Katsuyama, 1995*]. In the second type of OFDR, which requires a coherent source, the optical frequency itself is swept linearly with time. The back reflections are mixed with the launch radiation in the detector, to produce an optical-beat frequency. This heterodyne-frequency difference is proportional to the time delay between the source and reflecting event, and this, in turn, can be mapped into distance along the guided structure under test. This approach is capable of high resolution, and can be combined with coherent detection to produce good signal-to-noise ratio. Generally, these methods are more appropriate for characterizing discrete reflections (rather than distributed scattering), and are restricted to single-mode-waveguide structures.

The theoretical resolution of OFDR is given by

$$\Delta x = \frac{c}{N\Delta\omega}, \qquad (6)$$

where $\Delta\omega$ is the swept-frequency range. Spatial resolutions of 1-4 mm have been obtained for a laser diode, and 10 μm for a dye laser [*Glombitza and Brinkmeyer, 1993*].

Variations of this technique have also resulted in resolutions of around 10 μm [*Tanno et al., 1994*].

2.5.4 Reflectometry techniques: low coherence

Optical-low-coherence reflectometry (OLCR) is capable of the highest resolution reported to date (to a few micrometers), and is suitable for applications in the diagnostics of optical circuits and integrated-optical devices. Due to its importance in many fields, we will discuss OLCR in some detail. This method was developed independently, in 1987, by three research groups: [*Youngquist et al., 1987*], [*Danielson and Whittenberg, 1987*], [*Takada et al., 1987*]. Since then, a large number of applications of this technique have been reported, including measurements on transmission of optical circuits; dispersion of small optical components; polarization-mode dispersion; absolute optical ranging to 0.02 μm; timing characteristics of optical-fiber delay lines [*Danielson, 1993*]; backscattering, loss, and birefringence in optical waveguides and integrated-optical devices [*Takada et al., 1994*]; stability, loss, and dispersion in semiconducting lasers; characterization of fiber Bragg gratings [*Lambelet et al., 1993*]; photorefractive-phase conjugators [*Lambelet et al., 1994*]; and measurement of bending loss and optical-return loss in optical components. There is also much current interest in the study of biological tissues by OLCR methods [*Schmitt et al., 1993*]. Combination of OLCR with confocal microscopy is a promising new field that can be used for this purpose [*Schmitt, 1995*; *Izatt et al., 1994*]. Two recent survey articles may be consulted for additional references describing OLCR methods and applications [*Sorin et al., 1994*; *Gilgen, et al., 1993*].

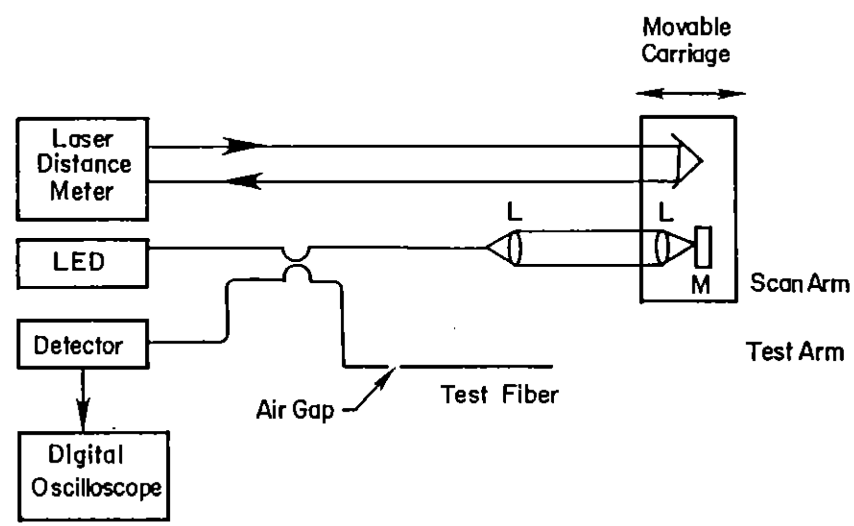

Figure 10. A low-coherence reflectometer for spatially locating discontinuities in fibers.

An example of an OLCR is shown in Figure 10. This configuration was designed for group-index measurements (see Section 2.5.5), but it can be used to illustrate most of the basic principles. The 3-dB fiber coupler defines the four arms of a scanning-Michelson interferometer with single-mode fibers. A source, such as an LED, that has a broad spectral width, is typically unmodulated. As the mirror is mechanically scanned, an interferogram is generated in the signal arm whenever the optical-path length, in the reference (scanning) arm, is equal (within the source-coherence length) to the optical-path length to a reflecting feature in the test arm. This is a form of homodyne detection. The signature can be used for diagnostic purposes, in ways similar to reflected pulses from a conventional OTDR. Due to the OLCR requirement for mechanical scanning, which is restricted to a limited range, this method is generally not suitable for systems with long lengths of fiber. However, OLCR has been adapted for accurate measurements of group delay in fibers the lengths of which are in excess of 1.5 km [*Danielson, 1993*]. *Baney and Sorin* [*1993*] have also developed a recirculating-delay-line method of increasing the effective optical-path scan distance.

The envelope of the interference pattern defines the theoretical resolution. For an optical source with Gaussian line shape that has a full width at half maximum (FWHM) of $\Delta\lambda$, the FWHM coherency envelope, Δx, is given by

$$\Delta x = \frac{2 \ln 2 \lambda^2}{\pi N \Delta\lambda}, \qquad (7)$$

with N, as before, being the group-refractive index of the waveguide. This relation applies to a single discrete reflection. LEDs are often used as optical sources, and the appropriate spectral profile in this case is approximately Gaussian.

Much attention is now being directed toward improving the performance of OLCRs, through the development of better optical sources, with characteristics including wavelength tunability, high power, and broad spectral width. Some of the novel sources yield resolutions around 2 μm or less, and provide enough optical power for large system dynamic ranges (reflection detection to -160 dB) [*Takada et al., 1993*; *Liu et al., 1993*; *Takada and Horiguchi, 1993*]. Synthesis of optical sources, through the mixing of multimode-laser diodes with slightly different wavelength characteristics, is another possibility that has generated considerable interest [*Rao et al., 1993*; *Wang et al., 1993*; *Wang et al., 1994*; *Kamatani and Hotate, 1993*; *Hotate and Kamatani, 1993*]. Mixing two superfluorescent optical-fiber amplifiers also shows promise [*Takada et al., 1994*; *Wysocki et al., 1994*].

Detection of backscattered radiation is difficult, under high-resolution conditions, using conventional pulsed-OTDR techniques. The OLCR cross-correlation signature can be compared, in a crude sense, to an "optical pulse" corresponding to the coherence time of the source (this analogy is not exact), and the same problem with signal amplitude exists here. That is, large system dynamic range is required to observe scattering in the

guided-wave structure. However, with considerable attention to detail, backscattering has been observed in integrated-optical devices using OLCR [*Takada et al., 1994*].

2.5.5 Group-index measurements in optical fibers

The reflectometry techniques that we have discussed so far actually measure group delay to a reflecting feature. In many cases, the desired information is physical distance to this feature. We can map delay into distance if we know the group index (at the operating wavelength of the reflectometer) of the transmission path over which the optical beam passes. In the case of commercial OTDRs, this index is entered into the instrument software by the user. Most modern OTDRs have four-significant-figure precision: that is, 1 plus four digits. Since most indices are around 1.46, this implies that a measurement precision around 0.00015 is possible. However, for the distance readout to have a comparable accuracy, a minimum requirement is for the group-index uncertainties of the fiber under test to be less than this figure. A concern for accurate OTDR distance measurements is our main motivation for obtaining precise optical-fiber group-index values.

OLCR methods provide us with a particularly convenient way for obtaining N for a long test fiber. Using this approach, relatively short samples can be taken for measurement from the ends of the much longer fiber which we wish to evaluate. Two different measurements need to be made on each of these short (about 5 cm) fiber samples. The physical length, L, is measured with a traveling microscope, calibrated with NIST gauge blocks. The group delay, T, is then measured using OLCR techniques. The ratio of these two quantities, multiplied by the velocity of light, gives the group index, or $N = cT/L$.

Figure 10 illustrates a low-coherence interferometer used at NIST for obtaining the group delay of the samples. The system incorporates two mechanically coupled interferometers. The first is part of a commercial fringe-counting (632.8 nm) distance meter, which measures the travel of the carriage, on which is also mounted a cat's eye retroreflector for the 1310 nm fiber-Michelson interferometer. The low-coherence source is an LED, with a spectral width of approximately 60 nm FWHM. The carriage has a travel in excess of 10 cm. Interferograms are generated by scanning the carriage around the point of equal optical-path lengths in the two arms. Fresnel reflections identify the ends of the fiber sample in the test arm, as indicated in Figure 11. Coarse adjustments of the carriage position are made manually and with a micrometer; the fine scan is produced by a calibrated PZT transducer. The group delay, T, is then obtained from the relation $T = N_a L/c$, where L is the measured travel between reflections on the distance meter, c is the velocity of light, and N_a is the group index of air at the central wavelength of the LED spectrum.

The sample fibers are butt-aligned with the launch fiber, with a three-axis micropositioner, at the input end. A small air gap is always maintained between the two fibers. Both single-mode and multimode fibers can be accommodated with this arrangement. With the multimode fibers, only the lowest-order on-axis-mode groups are excited, so they behave much like a single-mode fiber.

The uncertainty for the group-index measurements obtained from this system is about 0.06 percent (approximately two standard deviations).

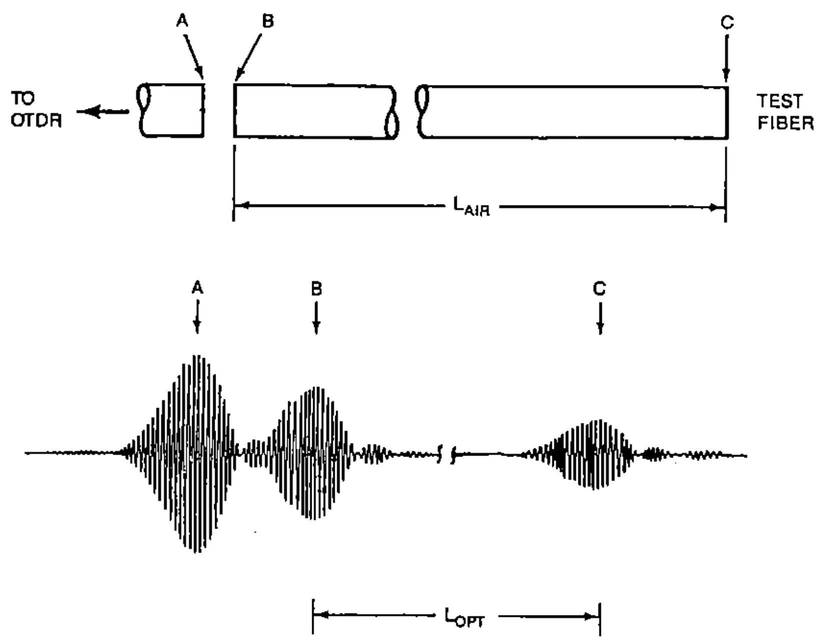

$$N = \frac{L_{AIR}}{L_{OPT}}$$

Figure 11. Typical fringe patterns from a low-coherence reflectometer, showing the locations of fiber-end faces (A, B, and C).

2.5.6 Standards for group index and OTDR calibration

A document entitled "Calibration of Optical Time-Domain Reflectometers" is currently (1995) under review by the IEC. It contains a detailed listing of OTDR-related definitions, calibration-test procedures, and methods of statistical analysis. These recommended standards should be published by the IEC in mid-1996. As far as distance-measuring accuracy goes, the test procedures relate only to instrumental-timing accuracy. The value of N which is appropriate to the fiber system under test must be entered manually into the OTDR device software. Although we feel that group index is one of the more important parameters necessary for the proper characterization of fibers and optical components, there are now no standards groups planning to establish preferred measurement techniques for N. Perhaps some of the experimental techniques referred to here can form the basis for such future standards.

3. Absolute optical-power measurements

Quantitative knowledge about the laser radiation transmitted through or emitted from optical-fiber-based optoelectronic systems is crucial to understanding these systems and their effective use. For telecommunications, power measurements are performed at the nominal wavelength regions of 850, 1300, and 1550 nm. However, for other applications (optical data storage, recording, etc.), shorter wavelengths (670 and 780 nm) can also be important. Although simple in principle, optical-power measurements can be difficult to accomplish accurately, because of numerous potential error sources [*Hentschel, 1989*]. In fact, a round robin, conducted in the early years of optical-fiber-power measurements, showed as much as a 20% variation among optical-power measurement laboratories [*Gallawa and Yang, 1986*]. Optical power can be measured using a collimated (or parallel) beam, but usually the radiation is transmitted through a fiber attached to the detector by a connector and adapter. The proximity of the fiber and connector to the detector and associated window provide an opportunity for reflections to introduce further errors in the power readings [*Gallawa and Li, 1987*; *Stock, 1990*]. Another property inherent in optical-power measurements is the effect of wavelength on the power readings. Since the wavelengths of diode lasers are not identical from laser to laser, the laser's spectral output, and the spectral responsivity of the detector, must be known.

Optical-power meters are probably the most common type of test equipment used to support optoelectronic systems. Detectors used for measuring optical power are generally divided into two basic types: thermal and quantum [*Dereniak and Crowe, 1984*]. Thermal detectors produce a signal in response to a radiation-induced temperature change proportional to optical power. Quantum detectors, on the other hand, produce an electrical signal proportional to the number of the incident photons absorbed per second. Each type (thermal or quantum) has specific advantages and disadvantages, but quantum detectors are, by far, more prevalent, because of their speed and sensitivity.

Thermal detectors usually contain a highly absorbent material (black paint, gold-black coating, etc.) onto which the optical radiation is incident. Absorption of the radiation results in conversion of the electromagnetic energy into thermal energy. The resulting temperature change is sensed by temperature sensors, such as thermocouples, which subsequently produce an electrical signal proportional to the temperature difference between the absorption structure, and a reference point elsewhere in the detector. Thermal detectors using thermocouples connected in series are called thermopile detectors. However, the most frequently used thermal detector for optical-power measurements is the pyroelectric detector. These devices are sensitive to the rate of temperature change and, thus, require modulated input to produce a signal. Pyroelectric detectors are sensitive to lower optical power than other types of thermal detectors and, consequently, are the most desirable thermal detectors for optical-fiber-power measurements. Thermal detectors are sometimes used as laboratory standards, because they are spectrally insensitive, have low reflectance, and can be calibrated electrically.

Quantum detectors (also called photodiode detectors), however, offer high speed and better detectivity (signal-to-noise) and, as a result, are the predominant type of detector used for measuring optical power. The electrical properties of quantum detectors change upon absorption of photons as electron-hole pairs are created: the degree of this change is related to the power of the incident radiation. Most quantum detectors used for optical-power measurements are made from photodiode sensors of silicon (Si), germanium (Ge), or indium gallium arsenide (InGaAs). Each of these diode-detector types is wavelength-sensitive, and thus is suitable for specific wavelength regions.

Due to manufacturing limitations, laser diodes do not operate at specific, well-defined wavelengths (or central wavelengths for multimode lasers), but typically emit radiation that is within ±10 nm of some desired value. Factors such as temperature can also cause the wavelength profile to change. Consequently, detectors that are spectrally sensitive (like diode detectors) can produce different outputs, when exposed to equal powers from different diode lasers, or even the same laser under different operational conditions. Naturally, to perform accurate measurements, both the spectral responsivity of the detector, and the spectral profile of the radiation emitted by the laser diode, must be characterized.

To support the industrial need for high-accuracy optical-power measurements, NIST has developed an optical-power-measurement system. As a primary reference standard, this system uses a thermal calorimeter which, in turn, is used to calibrate a transfer standard, using a characterized beamsplitter system and various laser sources. The transfer standard is then used with a measurement system specifically designed for optical-fiber-power measurements.

3.1 Primary reference standard

The most accurate type of detector now being used as an optical-power primary reference standard is the cryogenic radiometer [*Martin et al., 1985*; *Varpula et al., 1989*; *Foukal et al., 1990*]. These devices belong to a class of thermal detectors known, generically, as electrical-substitution radiometers (ESRs), in which electrical power is alternated with (or substituted for) optical power. The electrical power is applied through a resistive heater when the optical power is blocked, and is adjusted until the associated heating matches that from the optical input. The ESR is designed so that a given electrical power generates the same thermal response as would be produced from optical radiation at that same power. Differences in detector response, due to these two forms of heating (electrical and optical), are a major source of error for ESRs. Room temperature ESR devices are limited to absolute uncertainties in the range ±0.5-1%, due to the optical-

electrical inequivalence and other thermal-error sources. If the ESR is cooled to around 5 K, then the thermal diffusivity (the thermal conductivity divided by the specific heat capacity) of the cavity becomes approximately 1000 times as great. Consequently, many of the thermal error sources become negligible, and uncertainties in the range ± 0.005-0.01% are achievable. According to a survey taken at the September, 1994, meeting of the Consultative Committee on Photometry and Radiometry (CCPR), held in Paris, there are now at least ten national laboratories using cryogenic radiometers as primary standards for radiometric measurements.

Cryogenic radiometers normally contain a cylindrical absorbing cavity (made of thin-walled copper), the temperature of which is stabilized and controlled at about 5 K. The inside surface of the cavity is covered with a black paint that is highly absorptive in the visible- and near-infrared-wavelength region [*Stock and Hofer, 1993*]. The cavity is thermally connected to a heat sink immersed in a bath of liquid helium at 4.2 K (2 K, in some cases). Optical radiation absorbed by the cavity creates a temperature gradient between the cavity and the heat sink. Temperature sensors monitor this thermal gradient, and produce an electrical output proportional to the temperature difference. Resistive heaters are attached to the cavity, so that electrical power can be used to calibrate the response of the detector. Superconducting wires are used for the electrical leads going to the heater, so that no energy is dissipated in these wires.

In this low-temperature region (5 K), the thermal conductivity and heat capacity of the copper cavity vary rapidly with temperature; thus, the output response is nonlinear with respect to the incident radiation. This nonlinearity is calibrated with the electrical-substitution measurements, but still forces the radiometer be used in a steady-state mode. As a result, high-accuracy measurements require the use of a laser-power stabilizer, positioned in front of the radiometer. The absorbing-cavity structure is operated in a vacuum so that convective heat transfer is eliminated; consequently, a window is required at the entrance port to the radiometer. The window, usually made of high quality fused silica, is oriented at Brewster's angle relative to the incident laser beam, so that radiation polarized (from the laser-power stabilizer) with its electric field parallel to the plane of incidence has minimal reflectance.

Cryogenic radiometers have now been in use for approximately ten years. Their behavior has been well studied, and they are now widely accepted in the optical-power-measurement community. Although capable of high accuracy, they are difficult to use on a daily basis, because they require liquid helium, highly stable lasers, etc. A more "user friendly," mechanically cooled, cryogenic radiometer has been recently developed at the UK National Physical Laboratory (NPL), and it is now being used as their primary reference standard for optical power. Although it operates at 15 K, as opposed to 5 K, the stated uncertainty is still around ± 0.005%. However, the higher operating temperature, and the mechanical noise from the associated compressor, will need further study before the radiometer gains widespread acceptance. Only one such system is now in operation.

NIST is currently establishing a cryogenic primary standard for calibrations performed at its Boulder laboratory. The primary reference standard is now the C-series calorimeter [*West et al.*, *1972*; *West and Case*, *1974*]. This calorimeter was designed to accurately measure the electromagnetic radiation produced by CW (continuous wave) laser sources in the power range 1 mW to 1 W. The calorimeter was constructed to accommodate the unique characteristics of laser radiation (for example, nonuniform-intensity profiles, temporal and spatial coherence), and can be used over a wide wavelength range. It has proven to be a very cost effective, robust standard, capable of calibrating transfer standards with acceptable uncertainty. The calorimeter has a relatively simple geometrical structure (see Figure 12), and its behavior can be analyzed straightforwardly using first principles of thermodynamic analysis of linear systems.

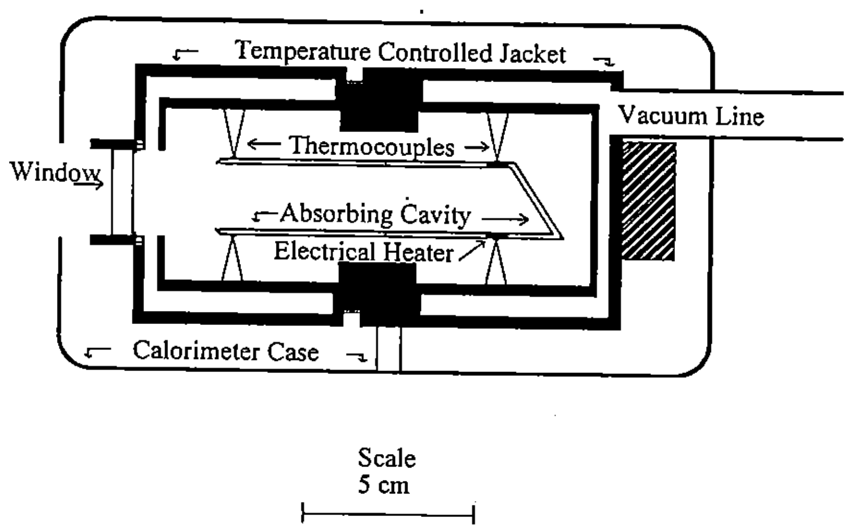

Figure 12. A C-series calorimeter.

The fundamental mechanism on which the operation of the calorimeter is based is the complete absorption of the laser radiation, with subsequent (and immediate) conversion of the electromagnetic energy to thermal energy. The energy absorption takes place in a cylindrical cavity, which is surrounded by a massive temperature-controlled jacket. Thermocouples, the junctions of which are bonded to both the absorbing cavity and the surrounding jacket, produce a thermoelectric voltage proportional to the temperature difference between these two structures. An electrical-heater wire is located in the absorbing cavity, to provide a means to calibrate the cavity electrically. The calorimeter was designed to maximize the equivalence between electrical and laser-energy deposition.

The absorbing-cavity structure actually consists of two cavities, one surrounding the other, approximately 1 mm away. These two thin-walled-copper cavities are thermally

joined by a copper connecting ring at their midsections. Thermocouple junctions are located at the ends of the outer cavity, and an electrical-heater wire is wrapped around the back end of the inner cavity. The inside surface of the inner cavity is coated with a flat black paint, which has an absorptance of about 97-98% over the visible-to-near-infrared-wavelength regions. The outer surfaces of the cavities, as well as the inner surface of the surrounding temperature-controlled jacket, are gold-plated, to reduce and stabilize the radiative-heat transfer, which occurs during a measurement. To eliminate convective-heat transfer, which can lead to nonlinear behavior under certain conditions, the calorimeter structure is evacuated to a pressure of around 10^{-6} Pa (10^{-8} Torr). A fused-silica window is located at the front aperture of the calorimeter. The window is wedged to prevent interference from affecting its transmittance.

During a laser measurement, the incident radiation passes through the window, and strikes the black paint on the back wall of the calorimeter. The paint absorbs most of the radiation at that point, and diffusely scatters the 2-3% not absorbed. The back wall is angled at 60°, so that any specular component is reflected to the side wall. Due to the length (10 cm) of the cavity relative to its diameter (2 cm), most of the diffusely scattered radiation is absorbed along the walls, leaving only a negligible amount to escape out through the window (less than 0.01% of the incident power). The heat generated in a circular area of paint at the back wall then spreads by conduction (primarily) throughout the inner cavity, and then through the connecting ring to the outer cavity. Eventually it reaches the thermocouple junctions at the ends of the outer cavity, and produces a corresponding thermoelectric voltage. This voltage is monitored with a digital voltmeter during the entire measurement process, and this acquired voltage information is used to calculate the amount of laser radiation absorbed by the cavity structure.

As evident from the design of this instrument, it is a heat-storage calorimeter, as opposed to a heat-conduction calorimeter (more commonly called power meter) and, consequently, has a very long time constant (≈12 min). Voltage readings are sampled once per second (nominally) during the measurement period, which may last about 10 min. This long time constant helps maximize the equivalence between electrical and laser-energy measurements, since it gives the heat more time to equilibrate within the calorimeter, before it is lost to the surroundings.

The system shown in Figure 13 is used to compare other detectors to the primary-standard C-series calorimeters. The beamsplitter is a 2° wedge, made of sapphire, with no optical coatings. A small angle of incidence (≈1°) of the incident beam, relative to the beamsplitter, minimizes the effects of polarization changes, and small changes in the angle of incidence, itself. The index of refraction of the sapphire is near 1.75, so the ratio of power in the transmitted beam to the reflected beam is approximately 11; a more exact value is used depending on the specific wavelength. The beamsplitter is calibrated at each specific wavelength, using two C-series calorimeters, to measure the power ratio of the two beams. The beamsplitter allows simultaneous measurements from both meters, and thus minimizes errors due to laser stability.

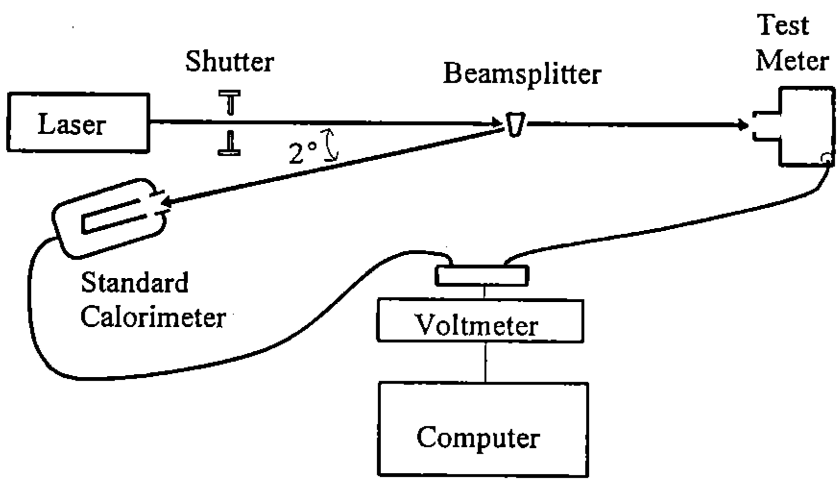

Figure 13. A C-series laser-measurement system.

A computer-controlled shutter is used to regulate the exposure time of the two instruments (the C-series calorimeter and the test meter), during the measurement. When the shutter is open and the laser energy is incident on the two detectors, voltage readings from both instruments are recorded. The C-series voltage information is used to determine the amount of energy incident onto the calorimeter. Then, using the beamsplitter ratio, the energy incident onto the test meter is calculated. The average power is found by dividing the energy by the exposure time. In some instances, intensity-stabilized lasers are used, to provide constant power to the test meter.

3.2 Measurement system for optical-fiber power meters

The device presently used as a transfer or laboratory standard for optical-power calibrations is a commercially available, electrically calibrated pyroelectric radiometer (ECPR) [*Phelan and Cook, 1973*]. The pyroelectric sensor is made of lithium tantalate, and is covered with a gold-black coating. The gold-black coating (≈ 1 μm thick) is pure gold, which has been evaporated and then deposited at a specific temperature and pressure, onto the lithium-tantalate surface. When deposited in this manner, the gold forms small, interwoven strands, which trap incident light. Gold-black is a common absorber for thermal detectors, and is approximately 99% absorbent [*Wolfe and Zissis, 1985*] in the visible and near-infrared regions. Because pyroelectric detectors require a modulated-optical input, a rotating chopper wheel is placed in front of the ECPR, when making measurements.

Before the ECPR is used as a transfer standard, it is first calibrated against the C-series calorimeters at a number of laser wavelengths, using the C-series-beamsplitter

system shown in Figure 13. After calibration, the ECPR is then used as the reference standard for optical-power measurements, which are performed using the system shown in Figure 14. The system contains several laser source plates, a connector-converter stage (for "connectorized" measurements), lenses (for parallel-beam measurements), and a positioning stage, for comparing the ECPR and the test meter which is being calibrated. All system optical fibers are single-mode, whereas the customer's fiber may be either single-mode or multimode. Each laser-source plate contains a laser diode, the output of which is transmitted through a fiber to a fiber splitter, from which about 1% of the energy travels through a fiber to a monitor detector. The remaining 99% goes to the meter being calibrated. Mandrel wraps are used throughout the system to help stabilize the power input to the detectors, and all fibers are securely fixed so that they will not move during the measurements.

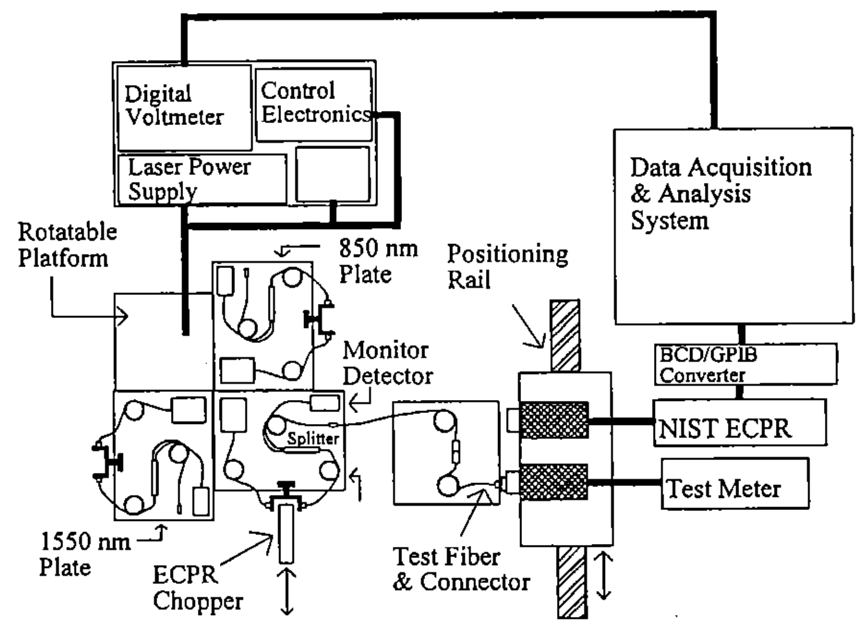

Figure 14. The optical-power-measurement system.

As shown in the figure, a U-shaped collimator fixture is positioned in the propagation path, following each diode laser. This fixture contains two lenses, which provide an open collimated beam for the ECPR chopper wheel. A sample-and-hold current-to-voltage converter is used for the monitor-detector output. This converter stores the voltage reading from the chopped signal, until the digital voltmeter takes a reading. For parallel-beam measurements, a lens at the end of the fiber path provides a collimated beam to the ECPR and test meter. For connectorized measurements, the customer's fiber is coupled to the measurement-system fiber, using a connectorized jumper-fiber assembly, located on a connector-converter stage. Power changes (due to diode-laser instability) are taken into account by the monitor-detector readings. The fiber-splitter ratio is measured before and after each set of measurements. Thus, this method relies on the stability of the splitter ratio, not on its actual value (as does the C-series measurement system).

Using this system, NIST offers measurement services for absolute-power calibrations of absolute-power meters (listed in the Laser Power and Energy section of NIST Special Publication 250). To supplement these measurements, NIST also offers Special Test measurements for linearity, spectral responsivity, uniformity, and frequency response of optical detectors.

3.3 Interlaboratory comparisons

One method of verifying accuracy and consistency among optical-power-measurement laboratories is through interlaboratory comparisons. Over the past ten years, several national and international intercomparisons have been completed, and all but the first have shown good agreement among participants.

An early optical-power round robin, conducted by NIST [*Gallawa and Yang, 1986*], showed large discrepancies among power-measurement laboratories in the US. At that time, optical-power measurements in the 850, 1300, and 1550 nm wavelength regions were relatively new. In addition, available detectors were not always of high quality. In this round robin, eleven participants in the US each calibrated a cooled-Ge detector (5 mm diameter), and sent the results to NIST for analysis. The measurements were performed at 850 and 1300 nm. The results at 850 nm showed a 6% standard deviation, and those at 1300 nm gave a 17% standard deviation. These large variations apparently resulted from using small-area detectors, which some of the radiation may have missed. Also, spatial non-uniformity of the detectors could have contributed to the sizable inconsistencies evidenced in that intercomparison.

Over the next five years, the quality of optical detectors improved substantially, and metrologists became more proficient at performing optical-power measurements. In 1990-1991, four national laboratories (US, UK, Germany, and Australia) participated in a pilot international intercomparison of optical power at 800, 850, 1300, and 1550 nm [*Gallawa, et al., 1991a*; *Gallawa et al., 1991b*]. Again, Ge photodiodes were used as the transfer standards, and were calibrated by the participating measurement laboratories. The data were compiled and analyzed by NIST. The results of these measurements showed excellent agreement between the laboratories, with a maximum difference between any two laboratories of 0.36% at 1330 and 1550 nm. At 800 and 850 nm, the results still showed good agreement, but a slightly larger maximum difference of 1.2% existed between any two laboratories; it is noted that Si photodiodes would be the better choice for transfer standards in this spectral range. The positive results of this intercomparison pilot effort provided the impetus to perform a larger, more-inclusive intercomparison.

In 1991-1992, an international measurement comparison of optical power was conducted among national laboratories from 13 countries [*Gardner et al., 1992*], including the four from the pilot program discussed above. Three Ge photodiodes were circulated among the laboratories for calibration measurements, and the results were collected and analyzed at NIST. Based on some calibrations of these detectors over the wavelength regions of 1270-1330 nm and 1520-1580 nm, in 5 nm increments, the data were normalized to 1300 and 1550 nm, as appropriate. The results showed variations of the order of 0.5% among the individual detectors at each laboratory, and differences of the order of ±1% between laboratories.

In the US, an optical-power round robin was conducted, with sponsorship of the National Conference of Standards Laboratories (NCSL), among nine optical-power-measurement laboratories, in industry and the military. A commercial Ge detector was sent to each participant for calibration, using a collimated beam at 1302 nm. The results of this intercomparison showed a standard deviation around 1%. A second phase of the round robin was then conducted in 1993-1994, in which a Ge detector was calibrated at 1300 and 1550 nm by 16 participants. In this round robin, the measurements were accomplished using a fiber with an FC connector. All previous intercomparisons discussed above were performed with collimated beams, thus avoiding the effects of connectors [*Gallawa and Li, 1987*]. Since most optical-power measurements are done with fibers and connectors, this round robin was more applicable to average power meter use. The results of this round robin also showed a standard deviation of around 1%.

The optical-power intercomparisons show that laboratories around the world, as well as in the US, are capable of accurate and consistent measurements on optical-power detectors. This is a significant improvement, compared to the state of measurement capability demonstrated in the 1985 intercomparison.

4. References

(Natl. Inst. Stand. Technol. publications referenced in this chapter are available from the Superintendent of Documents, US Government Printing Office, Washington, DC 20402.)

W. T. Anderson, V. Shah, L. Curtis, A. J. Johnson, and J. P. Kilmer [1987], "Mode-Field Diameter Measurements for Single-Mode Fibers with Non-Gaussian Field Profiles," *J. Lightwave Technol.*, **LT-5**, 2, pp. 211-217.

M. Artiglia, A. Chiantore, G. Ferri, and A. Rossaro [1994], "OTDR Trace Analysis for Fibre Characteristics Evaluation: a Bi-Directional Approach," *Technical Digest, Symposium on Optical Fiber Measurements*, Natl. Inst. Stand. Technol. Special Publication 864, pp. 61-64.

J. G. N. Baines, A. G. Hallam, K. W. Raine, and N. P. Turner [1990], "Fiber Diameter Measurements and Their Calibration," *J. Lightwave Technol.*, **8**, 9, pp. 1259-1268.

J. G. N. Baines, C. Freehill, and K. Raine [1994], "Fiber Diameter from Backscattered Light Pattern," *Technical Digest, Symposium on Optical Fiber Measurements*, Natl. Inst. Stand. Technol. Special Publication 864, pp. 125-128.

D. M. Baney and W. V. Sorin [1993], "Extended-Range Optical Low-Coherence Reflectometry Using a Recirculating Delay Technique," *IEEE Photon. Tech. Lett.*, **5**, 9, pp. 1109-1112.

M. Barnoski, M. D. Rourke, S. M. Jensen, and R. T. Melville [1977], "Optical Time Domain Reflectometer," *Appl. Opt.*, **16**, 9, pp. 2375-2379.

A. J. Barlow and I. Mackenzie [1987], "Direct Measurement of Chromatic Dispersion by the Differential Phase Technique," *Technical Digest, Optical Fiber Communication Conference*, paper TUQ1, Jan. 19-22, Reno, Nevada.

C. Brehm, O. Mercereau, G. Lipinski, and G. P. Vailleau [1994], "Contact and Non-Contact Interferometry for Optical Fiber Diameter Measurement and Calibration," *Technical Digest, Symposium on Optical Fiber Measurements*, Natl. Inst. Stand. Technol. Special Publication 864, pp. 133-136.

N. A. Brilliant, B. K. Alpert, and M. Young [1994], "Video Microscopy Applied to Optical Fiber Geometry Measurements," Natl. Inst. Stand. Technol. Tech. Note 1369.

A. Chiantore, G. Ferri, M. Artiglia, and P. DiVita [1994], "Comparison of Algorithms for Evaluating Fibre Attenuation Longitudinal Uniformity," *Technical Digest, Symposium on Optical Fiber Measurements*, Natl. Inst. Stand. Technol. Special Publication 864, pp. 69-72.

L. G. Cohen and C. Lin [1978], "A Universal Fiber-Optic (UFO) Measurement System Based on a Near-IR Fiber Raman Laser," *IEEE J. Quantum Electron.*, **QE-14**, 11, pp. 855-859.

A. Collyer, K. W. Raine, and J. G. N. Baines [1991], "Investigation into the Use of a Scanning Confocal Microscope as a Primary Measurement Method for Determining Optical Fibre Diameter," *Technical Digest, Optical Fibre Measurement Conference*, York, UK, Sept. 17-18, pp. 143-146.

S. A. Cooper and J. L. Hepburn [1993], "Approaches to Coating Diameter Calibration," *Technical Digest, Second Optical Fibre Measurement Conference*, Torino Italy, Sept. 21-22, pp. 53-56.

B. Costa, D. Mazzoni, M. Puleo, and E. Vezzoni [1982], "Phase Shift Technique for the Measurement of Chromatic Dispersion in Optical Fibers Using LEDs," *IEEE J. Quantum Electron.*, **QE-18**, 10, pp. 1509-1515.

B. L. Danielson and C. D. Whittenberg [1987], "Guided-Wave Reflectometry with Micrometer Resolution," *Appl. Opt.*, **26**, 14, pp. 2836-2842.

B. L. Danielson [1993], "Low-Coherence Interferometric Measurement of Group Transit Times in Precision Optical Fiber Delay Lines," *Technical Digest, Second Optical Fiber Measurement Conference*, Torino, Italy, pp. 159-162.

E. L. Dereniak and D. G. Crowe [1984], *Optical Radiation Detectors*, New York, John Wiley & Sons, pp. 23-183.

T. J. Drapela [1988], "Interlaboratory Comparison of Far-Field Methods for Determining Mode-Field Diameter using Both Gaussian and Petermann Definitions," *Technical Digest, Symposium on Optical Fiber Measurements*, Natl. Inst. Stand. Technol. Special Publication 748, pp. 179-181.

T. J. Drapela, D. L. Franzen, and M. Young [1994], "Fiber Geometry: Results of an International Interlaboratory Measurement Comparison," *Technical Digest, Symposium on Optical Fiber Measurements*, Natl. Inst. Stand. Technol. Special Publication 864, pp. 129-132.

K. A. Emig [1990], "A Comparison of Interferometric Techniques for Fiber Cladding Diameter Measurements," *Technical Digest, Symposium on Optical Fiber Measurements*, Natl. Inst. Stand. Technol. Special Publication 792, pp. 135-138.

P. V. Foukal, C. Hoyt, H. Kochling, and P. Miller [1990], "Cryogenic Absolute Radiometers as Laboratory Irradiance Standards, Remote Sensing, Detectors, and Pyroheliometers," *Appl. Opt.*, **29**, 7, pp. 988-993.

D. L. Franzen and R. Srivastava [1985], "Determining the Mode-Field Diameter of Single-Mode Optical Fiber: An Interlaboratory Comparison," *J. Lightwave Technol.*, **LT-3**, 5, pp. 1073-1077.

E. Frins, H. Failache, J. Ferrare, G. Da Cossta, and A. Lezama [1994], "Optical-Fiber Diameter Determination by Scattering at Oblique Incidence," *Appl. Opt.*, **33**, pp. 7472-7476.

R. L. Gallawa and Xiaoyu Li [1987], "Calibration of Optical Fiber Power Meters: The Effect of Connectors," *Appl. Opt.*, **26**, 7, pp. 1170-1174.

R. L. Gallawa and S. Yang [1986], "Optical Fiber Power Meters: A Round Robin Test of Uncertainty," *Appl. Opt.*, **25**, 7, pp. 1066-1068.

R. L. Gallawa, J. L. Gardner, D. H. Nettleton, K. D. Stock, T. H. Ward, and X. Li [1991a], "A Limited International Intercomparison of Responsivity Scales at Fiber Optic Wavelengths," *J. Res. Natl. Inst. Stand. Technol.*, **96**, 2, pp. 225-230.

R. L. Gallawa, J. L. Gardner, D. H. Nettleton, K. D. Stock, T. H. Ward, and X. Li [1991b], "Pilot Study for the International Intercomparison of Responsivity Scales at Fibre Optic Wavelengths," *Metrologia*, **28**, pp. 151-154.

A. Galtarossa, E. Nava, and G. Valentini [1993], "Measurements of Fiber Optics in Coherent Light," in Giovanni Cancellieri, *Single-Mode Optical Fiber Measurement: Characterization and Sensing*, Boston, Artech House, Chapter 4.

J. L. Gardner, R. L. Gallawa, K. D. Stock, and D. H. Nettleton [1992], "International Intercomparison of Detector Responsivity at 1300 and 1550 nm," *Appl. Opt.*, **31**, 34, pp. 7226-7231.

W. B. Gardner [1994], "Inter-laboratory Polarization Mode Dispersion Measurement Study," *Technical Digest, Symposium on Optical Fiber Measurements*, NIST Special Publication 864, pp. 171-174.

H. H. Gilgen, G. Bodmer, and Ch. Zimmer [1993], "Optical Coherence Domain Reflectometry as a Test Method for Integrated Optics Devices," *Technical Digest, Second Optical Fiber Measurement Conference*, Torino Italy, 1993, pp. 143-146.

N. Gisin, J. P. Von der Weid, and J. P. Pellaux [1991], "Polarization Mode Dispersion of Short and Long Single-Mode Fibers," *J. Lightwave Technol.*, **9**, 7, pp. 821-827.

U. Glombitza and E. Brinkmeyer [1993], "Coherent Frequency-Domain Reflectometry for Characterization of Single-Mode Integrated-Optical Waveguides," *J. Lightwave Technol.*, **11**, 8, pp. 1377-1384.

N. R. Haigh and T. C. E. Jones [1994], "The Development of an Optical Fibre Attenuation Standard," *Technical Digest, Symposium on Optical Fiber Measurements*, Natl. Inst. Stand. Technol. Special Publication 864, pp. 77-80.

P. D. Hale and D. L. Franzen [1992], "Fiber Cladding Diameter Measurement by White Light Interference Microscopy," *Technical Digest, Symposium on Optical Fiber Measurements*, Natl. Inst. Stand. Technol. Special Publication 839, pp. 51-58.

A. G. Hallam and J. H. Shaw [1992], "Measurement of Fibre Coating Geometry by Gray-Scale Analysis," *Technical Digest, Symposium on Optical Fiber Measurements*, Natl. Inst. Stand. Technol. Special Publication 839, pp. 59-62.

T. A. Hanson [1993], "Attenuation Uniformity Characterization," *Technical Digest, Second Optical Fibre Measurement Conference*, Torino, Italy, pp. 41-44.

B. L. Heffner [1992], "Automated Measurement of Polarization Mode Dispersion Using Jones-Matrix Eigenanalysis," *IEEE Photon. Technol. Lett.*, **4**, 9, pp. 1066-1069.

W. Heitmann [1987], "Precision Single-Mode Fiber Spectral Attenuation Measurement," *J. Opt. Commun.*, **8**, 1, pp. 2-8.

C. Hentschel [1989], "Making Accurate Fiberoptic Power Measurements", *Laser Focus/Electro-Optics*, September, pp. 108-119.

K. Hotate and O. Kamatani [1993], "Optical Coherence Domain Reflectometry by Synthesis of Coherence Function," *J. Lightwave Technol.*, **11**, 10, pp. 1701-1709.

J. A. Izatt, M. R. Hee, G. M. Owen, E. A. Swanson, and J. G. Fujimoto [1994], "Optical Coherence Microscopy in Scattering Media," *Opt. Lett.*, **19**, 8, pp. 590-592.

C. Joenathan and R. M. Bunch [1993], "Diameter Measurement of Single-Mode Fiber by Using Interferometric and Imaging Techniques," *Appl. Opt.*, **32**, 30, pp. 5989-5996.

O. Kamatani and K. Hotate [1993], "Optical Coherence Domain Reflectometry by Synthesis of Coherence Function with Nonlinearity Compensation in Frequency Modulation of a Laser Diode," *J. Lightwave Technol.*, **11**, 11, pp. 1854-1862.

K. C. Kao and G. A. Hockham [1966], "Dielectric-Fiber Surface Waveguides for Optical Frequencies," *Proc. IEEE*, **113**, 7, pp. 1151-1158.

F. P. Kapron, D. B. Keck, and R. D. Maurer [1970], "Radiation Losses in Glass Optical Waveguides," *Appl. Phys. Lett.*, **17**, 10, pp. 423-425.

Y. Katsuyama [1995], "In-Service Fiber Line Identification Based on High-Resolution Fiber Length Measurement," *J. Lightwave Technol.*, **13**, 1, pp. 6-13.

A. Klemas, W. A. Reed, D. S. Shenk, and M. Saifi [1985], "Analysis of Mode-Field Radius Calculated from Far-Field Patterns," *Technical Digest, Conference on Optical Fiber Communication*, paper TUB3, Feb. 13-14, San Diego, California, p. 30.

P. Lambelet, P. Y. Fonjallaz, H. G. Limberger, R. P. Salathe, Ch. Zimmer, and H. H. Gilgen [1993] "Bragg Grating Characterization by Low-Coherence Reflectometry," *IEEE Photon Tech. Lett.*, **5**, 5, pp. 565-567.

P. Lambelet, R. P. Salathe, M. H. Garrett, and D. Rytz [1994], "Characterization of a Photorefractive Phase Conjugator by Optical Low-Coherence Reflectometry," *Appl. Phys. Lett.*, **64**, 9, pp. 1079-1081.

H. H. Liu, P. H. Cheng, and J. Wang [1993], "Spatially Coherent White-Light Interferometer Based on a Point Fluorescent Source," *Opt. Lett.*, **18**, 9, pp. 678-680.

D. Marcuse [1981], *Principles of Optical Fiber Measurements*, New York, Academic Press, pp. 69-118.

J. E. Martin, N. P. Fox, and P. J. Key [1985], "A Cryogenic Radiometer for Absolute Radiometric Measurements," *Metrologia*, **21**, pp. 147-155.

S. Mechels and M. Young [1991a], "Video Microscope with Sub-Micrometer Resolution," *Appl. Opt.*, **30**, 16, pp. 2202-2211.

S. Mechels and M. Young [1991b], "Scanning Confocal Microscope for Precise Measurement of Optical Fiber Diameter," *Proc. Soc. Photo-Optical Instrum. Engrs.*, **1556**, pp. 164-170.

S. Mechels and M. Young [1992], "Scanning Confocal Microscope for Accurate Dimensional Measurement," *Proc. Soc. Photo-Optical Instrum. Engrs.*, **1660**, pp. 542-550.

W. Moller, K. Hube, D. Hunerhoff [1994], "Uncertainty of OTDR Loss Scale Calibration Using a Fiber Standard," *J. Opt. Commun.*, **15**, pp. 20-28.

M. S. O'Sullivan and D. W. Gransden [1987], "A Fizeau Fringe Interferometer for Fiber Outside Diameter Measurements," *Proc. Soc. Photo-opt. Instrum. Engrs.*, **841**, pp. 135-138.

A. J. Parker [1994], "Effect of Defocus on Near-Field Measurement of Fiber Mode Field Diameter," *Digest, 1994 Conference on Precision Electromagnetic Measurements*, June 27-July 1, Boulder, Colorado, pp. 499-500.

J. Parton [1988], "Improvements to the VAMFF System for Accurately Measuring the Mode-Field Diameter of Dispersion Shifted Fibers," *Technical Digest, Symposium on Optical Fiber Measurements*, Natl. Inst. Stand. Technol. Special Publication 748, pp. 183-186.

C. Pask [1984], "Physical Interpretation of Petermann's Strange Spot Size for Single-Mode Fibers," *Electron. Lett.*, **20**, 3, pp. 144-145.

S. D. Personick [1977], "Photon Probe–an Optical Time-Domain Reflectometer," *Bell Syst. Tech. J.*, **56**, 3, pp. 355-366.

K. Petermann [1983], "Constraints for Fundamental-Mode Spot Size for Broadband Dispersion-Compensated Single-Mode Fibers," *Electron. Lett.*, **19**, 18, pp. 712-714.

R. J. Phelan, Jr. and A. R. Cook [1973], "Electrically Calibrated Pyroelectric Optical-Radiation Detector," *Appl. Opt.*, **12**, 10, pp. 2494-2500.

C. D. Poole and D. L. Favin [1994], "PMD Measurements Based on Transmission Spectra Through a Polarizer," *J. Lightwave Technol.*, **12**, 6, pp. 917-929.

Y. J. Rao, Y. N. Ning, and D. A. Jackson [1993], "Synthesized Source for White-Light Sensing Systems," *Opt. Lett.*, **18**, 6, pp. 462-464.

G. Ripamonti, C. Riva, and A. Castoldi [1993], "Optimum Performance and Acquisition Methods for Single-Photon Optical Time-Domain Reflectometry," *Technical Digest, Second Optical Fiber Measurement Conference*, Torino, Italy, pp. 33-36.

M. J. Saunders [1988], "Non-Contact Interferometric Determination of the Outside Diameter of Optical Fibers," *Technical Digest, Symposium on Optical Fiber Measurements*, Natl. Inst. Stand. Technol. Special Publication 748, pp. 149-152.

J. M. Schmitt, A. Knuttel, and R. F. Bonner [1993], "Measurement of Optical Properties of Biological Tissues by Low-Coherence Reflectometry," *Appl. Opt.*, **32**, 30, pp. 6032-6035.

J. M. Schmitt [1995], "Compact In-Line Interferometer for Low-Coherence Reflectometry," *Opt. Lett.*, **20**, 4, pp. 419-421.

G. E. Smith [1990], "Measurement of Fiber Coating Geometry Using a Transversely Scanning Laser Beam," *Technical Digest, Symposium on Optical Fiber Measurements*, Natl. Inst. Stand. Technol. Special Publication 792, pp. 175-178.

D. H. Smithgall and C. M. Schroeder, "A Comparison of Techniques to Measure the Diameter of Lightwave Fiber," *Technical Digest, Symposium on Optical Fiber Measurements*, Natl. Inst. Stand. Technol. Special Publication 597, pp. 41-44.

W. V. Sorin, D. M. Baney, and S. A. Newton [1994], "Characterization of Optical Components Using High Resolution Optical Reflectometry Techniques," *Technical Digest, Symposium on Optical Fiber Measurements*, Natl. Inst. Stand. Technol. Special Publication 864, pp. 91-95.

K. D. Stock [1990], "Ge Photodiodes as Transfer Standards for Radiant Power Measurement in the Field of Fibre Optics," *Measurement*, **8**, pp. 31-35.

K. D. Stock and H. Hofer [1993], "Present State of the PTB Primary Standard for Radiant Power Based on Cryogenic Radiometry," *Metrologia*, 1993, **30**, pp. 291-296.

K. Takada, I. Yokohama, K. Chida, and J. Noda [1987], " New Measurement System for Fault Location in Optical Waveguide Devices Based on an Interferometric Technique," *Appl. Opt.*, **26**, 14, pp. 1603-1606.

K. Takada, and M. Horiguchi [1993], "Low Coherence Reflectometry Using Wavelength-Tunable Superfluorescent Fiber Source," *Electron. Lett.*, **29**, 14, pp. 1273-1275.

K. Takada, T. Kitagawa, M. Shimizu, and M. Horiguchi [1993], "High Sensitivity Low Coherence Reflectometer Using Erbium-Doped Superfluorescent Fiber Source and Erbium-Doped Power Amplifier," *Electron. Lett.*, **29**, 4, pp. 365-367.

K. Takada, H. Yamada, and M. Horiguchi [1994], "Diagnosis of Silica-Based Waveguides by Using a Jaggedness-Free OLCR," *Technical Digest, Symposium on Optical Fiber Measurements*, Natl. Inst. Stand. Technol. Special Publication 864, pp. 109-112.

N. Tanno, T. Ichimura, T. Funaba, N. Anndo, and Y. Odagiri [1994], "Optical Multimode Frequency-Domain Reflectometer," *Opt. Lett.*, **19**, 8, pp. 587-589.

M. B. van der Mark and L. Bosselaar [1994], "Noncontact Calibration of Optical Fiber Cladding Diameter Using Exact Scattering Theory," *J. Lightwave Technol.*, **12**, pp. 1-5.

T. Varpula, H. Seppa, J. M. Saari [1989], "Optical Power Calibrator Based on a Stabilized Green He-Ne Laser and a Cryogenic Absolute Radiometer," *IEEE Trans. Instrum. Meas.*, **38**, 2, pp. 558-564.

C. M. Wang, D. F. Vecchia, M. Young, and N. A. Brilliant [1994], "Software for Performing Gray-Scale Measurements of Optical Fiber End Faces," *Natl. Inst. Stand. Technol. Tech. Note 1370* (includes a computer disk in ANSI *FORTRAN* for computers with 80386 or higher processor).

D. N. Wang, Y. N. Ning, K. T. V. Gratten, A. W. Palmer, and K. Weir [1993], "Characteristics of Synthesized Light Sources for White-Light Interferometric Systems," *Opt. Lett.*, **18**, 22, pp. 1884-1886.

D. N. Wang, Y. N. Ning, K. T. V. Grattan, A. W. Palmer, and K. Weir [1994], "Optimized Multiwavelength Combination Sources for Interferometric Use," *Appl. Opt.*, **33**, 31, pp. 7326-7333.

K. H. Wanser and J. H. Anderson [1991], "Single-Mode Fiber Diameter Measurements Using Lloyd's Mirror," *Appl. Opt.*, **30**, 18, pp. 2422-2423.

E. D. West, W. E. Case, A. L. Rasmussen, and L. B. Schmidt [1972], "A Reference Calorimeter for Laser Energy Measurement," *J. of Res. Nat. Bur. Stand.*, **76A**, 1, pp. 13.

E. D. West and W. E. Case [1974] "Current Status of NBS Low-Power Laser Energy Measurement," *IEEE Transactions on Instrumentation and Measurement*, **M-23**, 4, pp. 422-425.

W. L. Wolfe and G. J. Zissis (eds.) [1985], *The Infrared Handbook*, prepared by the Environmental Research Institute of Michigan, ISBN:0-9603590-1-X pp. 7-79.

P. F. Wysocki, M. J. F. Digonnet, B. Y. Kim, and H. J. Shaw [1994], "Characteristics of Erbium-Doped Superfluorescent Fiber Sources for Interferometric Sensor Applications," *J. Lightwave Technol.*, **12**, 3, pp. 550-567.

M. Young, P. Hale, and S. Mechels [1993], "Optical Fiber Geometry: Accurate Measurement of Cladding Diameter," *J. Res. Natl. Inst. Stand. Technol.*, **98**, 2, pp. 203-216.

M. Young and R. C. Wittmann [1993], "Vector Diffraction by a Single-Mode Fiber: Application to Mode-Field Diameter Measurements," *Opt. Lett.*, **18**, 20, pp. 1715-1717.

R. C. Youngquist, S. Carr, and D. E. N. Davies [1987], "Optical Coherence-Domain Reflectometry: a New Optical Evaluation Technique," *Opt. Lett.*, **12**, 3, pp. 158-160.